An estimate of excess mortality resulting from air pollution caused by wildfires in the eastern and central Mediterranean basin in 2021

Bin Zhou[1] and Christoph Knote[1]

[1]University of Augsburg

November 23, 2022

Abstract

Wildfires result in human fatalities not only due to the direct exposure to flames, but also indirectly through smoke inhalation. The Mediterranean basin with its hot and dry summers is a hotspot for such devastating events. The situation has further been aggravated in recent years by climate change as well as a growing and aging population in the region. To assess the health impacts due to short-term exposure to air pollution created by the 2021 summer wildfires in the eastern and central Mediterranean basin, we used a regional-scale chemistry transport model to simulate concentrations of major air pollutants such as fine particulate matter with a diameter less than 2.5 µm ($PM_{2.5}$), SO_2, NO_2, and O_3 - in a fire and a no-fire scenario. Elevated short-term exposure of the population to air pollutants are associated with excess all-cause mortality using relative risks for individual pollutants from previously published meta-analyses. Our estimates indicate that the short-term exposure to wildfire-caused changes in O_3 accounted for 741 (95% CI:556-940) excess deaths in total over the entire region of investigation during the wildfire season between mid-July to early October 2021. This is followed by 270 (95% CI:177-370) excess deaths due to elevated $PM_{2.5}$ exposure, rendering the health effect of increased O_3 from wildfires larger than the effect of increased $PM_{2.5}$. We show this to be attributed largely to the spatially more widespread impact of wildfires on O_3. Our study concludes with a discussion on uncertainties associated with the health impact assessment based on different air pollutants.

An estimate of excess mortality resulting from air pollution caused by wildfires in the eastern and central Mediterranean basin in 2021

Bin Zhou[1,2], Christoph Knote[1]

[1]Model-based Environmental Exposure Science, Faculty of Medicine, University of Augsburg, Augsburg, Germany
[2]Potsdam Institute for Climate Impact Research (PIK), Member of the Leibniz Association, Potsdam, Germany

Key Points:

- Exposures to $PM_{2.5}$ and O_3 caused by 2021 summer wildfires accounted for 270 and 741 excess deaths in the eastern and central Mediterranean.
- Excess deaths attributable to increased O_3 exposure exceed those based on $PM_{2.5}$ exposure.
- Choice of exposure response functions leads to uncertainty up to a factor of 3.

Corresponding author: Bin Zhou, bin.zhou@med.uni-augsburg.de

Abstract

Wildfires result in human fatalities not only due to the direct exposure to flames, but also indirectly through smoke inhalation. The Mediterranean basin with its hot and dry summers is a hotspot for such devastating events. The situation has further been aggravated in recent years by climate change as well as a growing and aging population in the region. To assess the health impacts due to short-term exposure to air pollution created by the 2021 summer wildfires in the eastern and central Mediterranean basin, we used a regional-scale chemistry transport model to simulate concentrations of major air pollutants such as fine particulate matter with a diameter less than 2.5 μm ($PM_{2.5}$), SO_2, NO_2, and O_3 - in a fire and a no-fire scenario. Elevated short-term exposure of the population to air pollutants are associated with excess all-cause mortality using relative risks for individual pollutants from previously published meta-analyses. Our estimates indicate that the short-term exposure to wildfire-caused changes in O_3 accounted for 741 (95% CI:556-940) excess deaths in total over the entire region of investigation during the wildfire season between mid-July to early October 2021. This is followed by 270 (95% CI:177-370) excess deaths due to elevated $PM_{2.5}$ exposure, rendering the health effect of increased O_3 from wildfires larger than the effect of increased $PM_{2.5}$. We show this to be attributed largely to the spatially more widespread impact of wildfires on O_3. Our study concludes with a discussion on uncertainties associated with the health impact assessment based on different air pollutants.

Plain Language Summary

Wildfires lead to loss of life not only when directly affected, but also through the inhalation of the smoke generated. The Mediterranean basin is frequently affected by wildfires due to its hot and dry climate. Climate change as well as an increasingly aging population made matters worse. In this study, we estimate the loss of life caused by wildfires in the eastern and central Mediterranean basin in summer 2021. We used a computer model to simulate concentrations of air pollutants emitted from wildfires and estimate the resulting excess human deaths based on the most relevant evidence from literature. Our estimates found that wildfires account for several hundred excess deaths in the study region between mid-July to early October 2021. We estimate the effects of Ozone, a gaseous air pollutant, to exceed those of particles created by wildfires. Furthermore, we discuss the uncertainties associated with our estimates.

1 Introduction

Air pollution is a central issue in public health globally given its well-documented association with adverse health effects (Brunekreef & Holgate, 2002; Anenberg et al., 2010; Lelieveld et al., 2020). Exposure to air pollution, both long-term and short-term, is estimated to cause millions of premature deaths and lost years of healthy life each year (WHO, 2021). Air pollution from wildfires is becoming a subject of increasing concern due to the higher toxicity associated with its chemical composition (Naeher et al., 2007; Wegesser et al., 2009). Furthermore, smoke from wildfires can travel large distances and impact the health of a much larger population than the effects of the actual fire (Bencherif et al., 2020). Most recently, prominent examples are wildfires in the Amazon in 2019 (Butt et al., 2021), Australia in 2019-2020 (Graham et al., 2021), and those in the United States in recent years (Burke et al., 2021; Kramer et al., 2019; Xie et al., 2020). It has been shown that frequency and magnitude of fire events are increasingly affected by human activities and have been exacerbated by climate change (Bowman et al., 2020; Jolly et al., 2015).

Globally, wildfire smoke is estimated to cause more than 330,000 premature deaths each year during 1997 - 2006 (Johnston et al., 2012). As climate change worsens, together with updated evidence of impacts of wildfires on human health (Chen et al., 2021; Haikerwal et al., 2015), wildfires are projected to result in increased human and material losses in the near future (Xu et al., 2020). Furthermore, wildfires can lead to a higher susceptibility to other (respiratory) diseases, with reports of an amplified risk of COVID-19 cases and deaths in wildfire seasons (Zhou et al., 2021; Schwarz et al., 2022) as a prime example. This may imply that previous studies may systematically underestimate the actual health impacts of wildfires, as they fail to adequately address the underlying relationship between wildfires and other environmental and health concerns.

Historically, the Mediterranean basin which is characterized by hot and dry summers has been negatively affected by wildfires. With increased warming and declining precipitation, the Mediterranean basin is expected to experience an increase in the frequency and scale of wildfires (Ruffault et al., 2020; Cos et al., 2021). Meanwhile, the rapid population growth in some countries (e.g., Egypt, Israel, and Tunisia) and an ageing population in others (e.g., southern European countries) renders the Mediterranean basin ever more vulnerable to the unfavorable consequences of climate change (Linares et al., 2020). All this demands a comprehensive assessment of population exposure to wildfire-caused air pollution.

In this context, the 2021 summer wildfires in the eastern and central Mediterranean basin serve as an indicator of future wildfire impacts. In our work we used this case to assess the health impacts due to short-term exposure to air pollution from wildfire smoke. An online-coupled atmospheric chemistry transport model was employed to simulate concentrations of major air pollutants – fine particulate matter with a diameter of 2.5 μm or less ($PM_{2.5}$), SO_2, NO_2, and O_3 – in a fire and a no-fire scenario. Elevated short-term exposure to air pollutants are associated with excess all-age all-cause mortality using relative risks (RRs) for individual pollutants based on previously published meta-analyses. We estimated the excess mortality attributable to wildfires for the entire region and the countries included, with detailed discussions on the uncertainties associated with the estimates.

2 Data and Methods

2.1 Study area and period

The study area covers 18 countries and regions in the central and eastern Mediterranean basin with a total population of 334.62 million in 2020, of which over half resides along its coastal areas and hydrological basins (World Bank, 2020). For a full list of countries included in the study and their respective populations, please refer to Table S1 in the Supplementary Information (SI).

We used the UN WPP-Adjusted population count GPWv4 dataset of the Gridded Population of the World, Version 4 (GPWv4) data from the Socioeconomic Data and Application Center (SEDAC) for 2020 (CIESIN, 2018) to describe the spatial population distribution. From the original resolution of 2.5 arc-minute (approx. 5 km) data were aggregated to a grid of about 20 x 20 km^2 to be consistent with the configuration of the numerical model employed in this study (Fig. 1 a).

The study period was 15 July - 02 October 2021, covering the major wildfire events in summer 2021. The severe dry conditions and heatwaves prevailing in this period have resulted in many intense and long-lasting wildfires across the region, emitting large amounts of air pollutants (e.g., particulate matter, NO_x, and SO_2) into the atmosphere (CAMS, 2021). According to the European Forest Fire Information System (EFFIS) (EFFIS, 2021), there were more than 1800 wildfires with a burnt area of 10 hectares or larger occurring in the region and period of this study, which burnt 589,400 hectares area in total. As shown in Fig. 1 b-c, the worst hit countries include Turkey, Greece, Italy, Tunisia, and the ones in the Balkans (e.g., Albania, Montenegro, and North Macedonia).

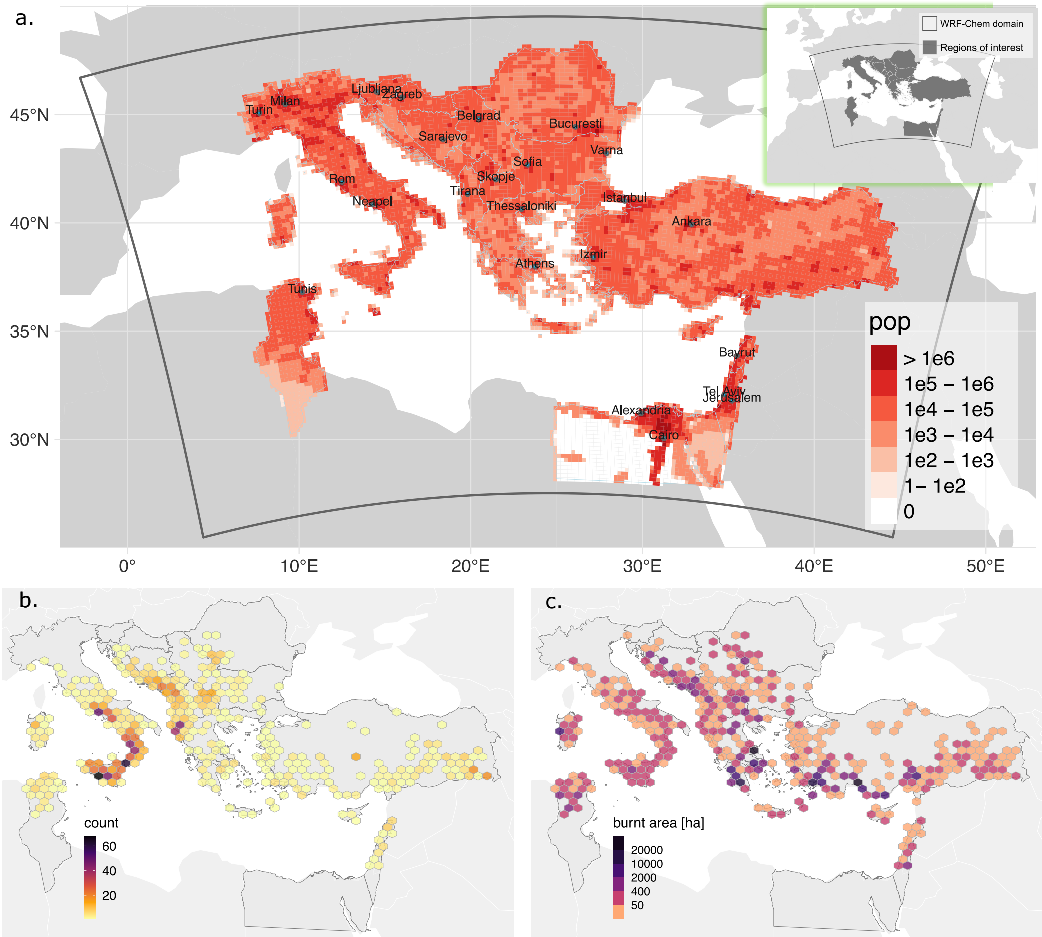

Figure 1. The study region overlaid with the population data and wildfire statistics. a) Population counts per country from the Gridded Population of the World, Version 4 (GPWv4) data for 2020 (CIESIN, 2018). The fan-shaped polygon demarcates the simulation domain. b-c) the total number of wildfires and total burnt areas, respectively, based on the European Forest Fire Information System (EFFIS) data between 15-July and 02-October, 2021. Countries included in the study are outlined in black.

2.2 Model description

Concentrations of $PM_{2.5}$, O_3, NO_2, and SO_2 were simulated using the Weather Research and Forecasting model coupled to Chemistry (WRF-Chem) model (version 4.2.1), a fully online-coupled regional atmospheric chemistry model (Grell et al., 2005). The Model for Ozone and Related chemical Tracers, version 4 (MOZART-4) gas-phase chemistry mechanism (Emmons et al., 2010) with considerable updates to the chemistry of volatile organic compounds (Knote et al., 2014) was used to predict trace gas concentrations. Aerosol characteristics were simulated with the 4 size-bin implementation of the MOSAIC aerosol module (Zaveri et al., 2008). This includes a simplified formulation of secondary organic aerosol formation (Hodzic & Jimenez, 2011), including that from wildfires. Analyses interlaced with hourly forecasts from the Global Forecasting System (GFS) of the National Centers for Environmental Prediction (NCEP) made available through the NOAA Operational Model Archive and Distribution System (NOMADS, (Rutledge et al., 2006)) were used as initial and boundary conditions for meteorological variables. Results of simulations of the Whole Atmosphere Community Climate Model (WACCM) model created by the Atmospheric Chemistry Observations & Modeling Laboratory (ACOM) of the National Center of Atmospheric Research (NCAR) served to provide initial and boundary conditions for trace gases and particles (`https://www.acom.ucar.edu/waccm/`, last accessed 02.03.2022). The EDGAR-HTAP dataset was used for prescribing anthropogenic emissions (Janssens-Maenhout et al., 2012). The model simulations also considered biogenic emissions from plants (Guenther et al., 2006), desert dust (LeGrand et al., 2019) and sea spray (Gong, 2003). Emissions of trace gases and particles from wildfires were included by the Fire INventory from NCAR (FINN) model (Wiedinmyer et al., 2011), based on daily observations of fire radiative power by the MODIS and VIIRS satellite instruments.

The model domain covers the central and eastern Mediterranean basin (1.47 - 47.63°E, 27.60 - 49.45°N) at 20 km horizontal resolution, with 33 vertical levels (up to 10 hPa) (Figure 1a). Two simulations, a fire and a no-fire scenario, were performed to quantify the contribution of wildfires to concentrations of major air pollutants. This model configuration has already been evaluated in different regions of the world and used to simulate the concentrations of various air pollutants (Graham et al., 2021; Butt et al., 2021).

2.3 Model evaluation

We used the European Environmental Agency (EEA)'s AirBase air quality (including $PM_{2.5}$, O_3, NO_2, and SO_2) time series data sets (E1a & E2a) to evaluate the WRF-Chem simulations. AirBase data reported by EEA's member states are provided either at hourly or daily intervals. Based on type and location, AirBase stations are classified as rural (including "rural-remote", "rural-regional"), sub-urban (including "rural-nearcity"), and urban. All AirBase data are quality-checked and flagged with different levels of verification (European Environment Agency, 2021). We only used data with "verification code" equal to 1 (verified) or 2 (preliminary verified) in the metadata, and only from stations where more than 75% of observations were present during the entire period. For stations where only daily means were recorded, hourly WRF-Chem values were averaged to daily means for comparison. The data were downloaded using `airbase 0.2.7` python library (`https://pypi.org/project/airbase/`).

2.4 Health impacts assessment (HIA)

Health impacts of short-term exposure to wildfire-caused air pollution were estimated using a well-established methodology (WHO, 2016). Details of the main steps are given below.

2.4.1 Determination of population exposure to air pollution

Population exposure was quantified for each country by calculating the population-weighted concentrations of air pollutants using GWPv4 population data and pollutant concentration data from the WRF-Chem simulations. For country J on day d, its population weighted exposure (Cpw) to a pollutant i - say, i is $PM_{2.5}$, is then calculated as:

$$Cpw^{i,J,d} = \frac{\sum_{\forall j \in J} (pop_j \times c_{ijd})}{\sum_{\forall j \in J} pop_j} \tag{1}$$

where c_{ijd} is the daily mean air pollutant concentration for $PM_{2.5}$, SO_2, and NO_2, whereas the daily mean 8 hour average (DMA8) is used for O_3. Population-weighted exposure was computed for both fire and non-fire scenarios, with their difference representing the additional health burden attributable to wildfires.

2.4.2 Estimate of exposure-associated health risk

To estimate the exposure-associated health risk, we used both baseline health statistics (here e.g., mortality) and an exposure-response-function (ERF) for individual air pollutants.

The baseline all-cause mortality data in both genders (deaths per annum) for 2019 (the latest year for which data are available) were downloaded from the Global Health Data Exchange (GHDx) (Global Burden of Disease Collaborative Network, 2020). To interpolate the annual deaths to the summer months (July-August-September) 2021, we used the multi-annual (2010-2019) average of monthly deaths as proxy. Monthly baseline mortality data are collected by the European Statistical Office (Eurostat) for its member and associated states (Eurostat, 2021). For countries where monthly deaths are not available, e.g., Tunisia, Israel, and Egypt, the monthly mean deaths averaged over all other countries in this region were used as proxy (Figure S2 in SI). Total monthly deaths were then equally distributed to each day of the month.

An ERF associates the proportional increase in exposure of an air pollutant with the potential adverse health outcomes, typically expressed as relative risk (RR). The RR is a ratio of incidences (e.g., deaths) exposed to air pollution relative to to incidences with no exposure. The RR can be estimated either by 1) pre-defined formulas or ranges of values from studies or meta-analyses, or 2) by integrated ERF approaches (Burnett et al., 2014; Cohen et al., 2017). Here, we chose the former approach, adopting RR values for short-term exposure mainly from a recently published systematic review by Orellano et al. (2020). To assess the uncertainty due to different RR estimates, we additionally calculated health impact estimates with RRs from different reviews published before (World Health Organization, 2013; Orellano et al., 2020; Vicedo-Cabrera et al., 2020; Liu et al., 2019). The RRs together with their respective 95% confidence intervals (CIs) are listed in Table 1.

Given a linear relationship and an exposure increase ΔC of 10 μg/m^3, the $RR_{\Delta 10}$ is defined as

$$RR_{\Delta C} = e^{\beta \Delta C}. \tag{2}$$

From Equation 2 we can back out the coefficient β and use it to estimate RRs for arbitrary ΔX:

$$RR(\Delta X) = e^{\beta(\Delta X - X_0)}, \tag{3}$$

where X_0 is the theoretical minimum risk exposure level, below which no additional risk is assumed. In line with previous works (Graham et al., 2021; Macintyre et al., 2016),

	Relative risk (95% CI)	
	$PM_{2.5}$	O_3
Orellano et al. (2020)	1.0065 (1.0044–1.0086)	1.0043 (1.0034–1.0052)
WHO (2013)	1.0123 (1.0045-1.0201)	1.0029 (1.0014-1.0043)
Liu et al. (2019)*	1.0068 (1.0059-1.0077)	–
Vicedo-Cabrera et al. (2020)	–	1.0018 (1.0012-1.0024)

* 2-day moving average is used as the exposure metric instead of the daily mean used elsewhere.

Table 1. Relative risks ($RR_{\Delta 10}$) with 95% confidence interval (CI) of all-cause mortality associated with short-term exposure to $PM_{2.5}$ and O_3 for an increase of 10 $\mu g/m^3$ concentration, obtained from selected meta-analysis or multi-city studies published before.

we assume X_0 to be zero. We then derived excess exposures to an air pollutant i emitted from wildfires as the difference in population exposure between the fire and no-fire simulations for a country J:

$$\Delta Ci, J = Cpw_{i,J}^{fire} - Cpw_{i,J}^{no-fire} \tag{4}$$

To account for the health impacts on the population level, the population attributable fraction (PAF), defined as the fraction of adverse health outcomes in a population attributable to a specific exposure, is computed using the formula (Mansournia & Altman, 2018):

$$PAF = 1 - \frac{1}{RR} \tag{5}$$

The excess number of deaths attributable to wildfire-caused exposure to air pollutant i for a country J within the entire period of simulation ($E_{i,J}$) is computed as:

$$E_{i,J} = \sum_{d=1}^{N} (BM_{J,d} \times pop_J \times PAF_{i,J}), \tag{6}$$

where $BM_{J,d}$ is the baseline mortality for the country J on day d, and N is the total number of days simulated.

2.4.3 Estimate of uncertainty due to error propagation in excess mortality

Numerous sources of uncertainty exist for such a health impact assessment which have been discussed in details elsewhere (WHO, 2016).

In this study, we accounted for the uncertainty arising from the multiplication of baseline mortality and relative risk, both of which are bounded with their respective 95% CIs. Assuming a normal distribution for both data sets ($x \sim \mathcal{N}(\mu, \sigma^2)$), the standard error (SE) of each data is derived as:

$$\mathrm{SE}(x) = (\mathrm{CI}^{\mathrm{upper}} - \mathrm{CI}^{\mathrm{lower}})/(2 \cdot z_{1-0.05/2}), \tag{7}$$

where $z_{1-0.05/2}$ is the 0.975 quantile of the standard normal distribution ($z_{0.975} \approx 1.96$). Then, the variance $\mathrm{Var}(x) = \mathrm{SE}(x)^2$. As PAF depends linearly on $1/RR$ (Equation 5), its SE and variance are linear derivatives of those for $1/RR$.

To quantify the propagation of the uncertainties in the excess mortality estimates, two approaches were used. The first approach is based on the delta method (Ver Hoef, 2012). For the product of baseline mortality and PAF (as in Equation 6), the joint standard error is calculated below:

$$\mathrm{SE}(\hat{x_1}\hat{x_2}) = \sqrt{\hat{x_1}^2\mathrm{Var}(\hat{x_2}) + \hat{x_2}^2\mathrm{Var}(\hat{x_1}) + 2\hat{x_1}\hat{x_2}\mathrm{Cov}(\hat{x_1}, \hat{x_2})}, \tag{8}$$

where $\hat{x_1}$, and $\hat{x_1}$ represent the expectations of baseline mortality and PAF, respectively. Since baseline mortality and PAF are mutually independent, their covariance is zero. Equation 8 can be further shortened as:

$$\mathrm{SE}(\hat{x_1}\hat{x_2}) = \sqrt{\hat{x_1}^2\mathrm{Var}(\hat{x_2}) + \hat{x_2}^2\mathrm{Var}(\hat{x_1})} \tag{9}$$

The 95% confidence intervals for the product x_1x_2 are $\hat{x_1}\hat{x_2} \pm 1.96\mathrm{SE}(\hat{x_1}\hat{x_2})$.

The second approach is based on the Monte Carlo method. We respectively generated the normally distributed random samples of BM and PAF (with a sample size N = 1000) based on the expectations and SEs derived from Equation 7. The 2.5% and 97.5% percentiles of the sample composed of the element-wise product of BM and PAF designated the lower and upper bounds of the 95% CIs for their product. Repeating for 100 times, the respective mean values of lower and upper bounds quantified the uncertainty for the estimated health impacts.

We used the R software (version 4.1.1) (R Core Team, 2021) and the *sf* package (version 1.0-4) (Pebesma, 2018) to perform the statistical and geo-spatial analyses.

3 Results

3.1 Model validation

Figure S3-S4 in SI show normalized Taylor diagrams for $PM_{2.5}$ and O_3 simulations for rural, sub-urban, and urban AirBase stations. Subject to the collection frequency of AirBase data, the performance was evaluated for daily and hourly means, respectively.

Overall, WRF-Chem model performance is on par with recent multi-model intercomparison studies of air quality models over Europe and North America (Im et al., 2015b, 2015a) and produced accurate estimates for the concentrations of $PM_{2.5}$ and O_3 when compared to the AirBase dataset. We note that a perfect simulation, especially of urban stations cannot be expected due to the very different representativeness of station measurements and the 20 km horizontal resolution of WRF-Chem.

The estimates of $PM_{2.5}$ from the WRF-Chem simulations were marginally better for daily mean values than for hourly values when compared to the observations, whereas the performance exhibited no significant difference between stations of different types. The correlation coefficients between the simulated and observed concentrations (on polar axes) range from 0.5 to 0.7. By comparison, neither the averaging time (hourly vs. daily) nor the type of station affected the model performance in estimating O_3 concentration.

3.2 Effects of wildfires on health-relevant pollutant concentrations

Wildfires emit large amounts of particulate matter, nitrogen oxides (NO_x), as well as carbon monoxide (CO) and other volatile organic compounds (VOCs) into the atmosphere (Schneider & Abbatt, 2022). They increase $PM_{2.5}$ levels through direct emission of particles as well as the formation of secondary $PM_{2.5}$ from the oxidation of the emitted SO_2, NO_x, and VOCs. These species are oxidized to less volatile sulfates, nitrates, and secondary organic aerosols (SOAs), respectively, which then condense onto pre-existing particles or form new ones (Kroll et al., 2020). Some VOCs are in part emitted with semi- and low volatility and will condense onto particles upon dilution and cooling without the need of further photochemical reactions.

Increased NO_x and VOCs from wildfires lead to additional O_3 formation downwind through photo-chemical reactions (Jaffe & Wigder, 2012). In addition, wildfires can increase concentrations of the hydroxyl radical (OH), leading to an increased atmospheric oxidation capacity, which further favors the formation of secondary particulate matter.

3.3 Spatio-temporal patterns of air pollutant concentrations

Figure 2 a shows the spatial pattern of the WRF-Chem simulated $PM_{2.5}$ concentration as average over the entire period based on the fire scenario.

The mean $PM_{2.5}$ concentrations range from 5 to 160 $\mu g/m^3$ across the region. High $PM_{2.5}$ loads are clearly visible in regions that are already heavily polluted even in the absence of wildfires, e.g., along the eastern coastlines of Turkey including the metropolitan area of Istanbul, and the eastern Ukrainian metropolitan area of Mariupol on the north coast of the Azov sea. The latter region is one of the most polluted regions in Europe. Furthermore, urban areas exhibit faintly higher $PM_{2.5}$ concentrations in contrast to non-urban regions.

Figure 2 b and c show the spatial pattern of fires-caused $PM_{2.5}$ concentration relative to that under no-fires scenario, and the percentage of $PM_{2.5}$ loads attributable to wildfires. The increased $PM_{2.5}$ concentrations caused by wildfires are mainly observed in the Balkans, Greece, and southern Italy, coinciding with the distribution of fire events within the simulation period (Figure 1 b-c). Some regions with high background industrial pollution exhibit no change or even a slight decrease in ambient $PM_{2.5}$ concentration.

Diurnally, the $PM_{2.5}$ concentration is subject to the mixing layer height (Figure S8 in SI). The daytime troughs reflect strong turbulent exchange and dilution within the mixed layer, whereas stable nighttime boundary layer enables $PM_{2.5}$ to accumulate (Manning et al., 2018).

Figure 3 shows the spatial pattern of WRF-Chem-simulated O_3 concentrations. In contrast to the $PM_{2.5}$ pattern, the O_3 concentration demonstrates an upward gradient from urban agglomerations to non-urban surroundings, indicating titration by large urban nitrogen oxides (NO_x) emissions.

The overall effect of the wildfires on O_3 is more widespread due to the longer atmospheric formation and lifetime of O_3, and is hence visible on a country level (Figure S9). Interestingly, the border region between Bulgaria and Romania is observed to be one of regions most affected by wildfire-caused O_3 pollution, which may be accounted for by the location-specific topography and the fact that it is located downwind of a number of fires that occurred during the season. The region on the lower Danube plain is further bounded by the Carpathian Mountains to the North and West and by the Balkan Mountains to the South which forms a semi-closed topographical feature, channeling and concentrating air pollutants emitted from wildfires.

Figure S9 in SI shows the diurnal pattern of O_3, which is determined by the presence of sunlight, as O_3 is formed primarily by photo-chemical reactions.

Figures S5-S6 and S10-S11 in SI show the spatial and temporal pattern of NO_2 and SO_2 concentrations, respectively. The hot spots of NO_2 and SO_2 are principally found in cities, along artery roads and shipping routes (Figure S5), and in large point sources like power plants and oil and gas refineries (Figure S6 a).

By comparison to O_3, increases of NO_x and SO_2 are less visible on a country level (Figures S9-S10), as their effects are limited locally due to their relatively shorter atmospheric lifetime, and the dilution into comparatively high pre-existing background concentrations.

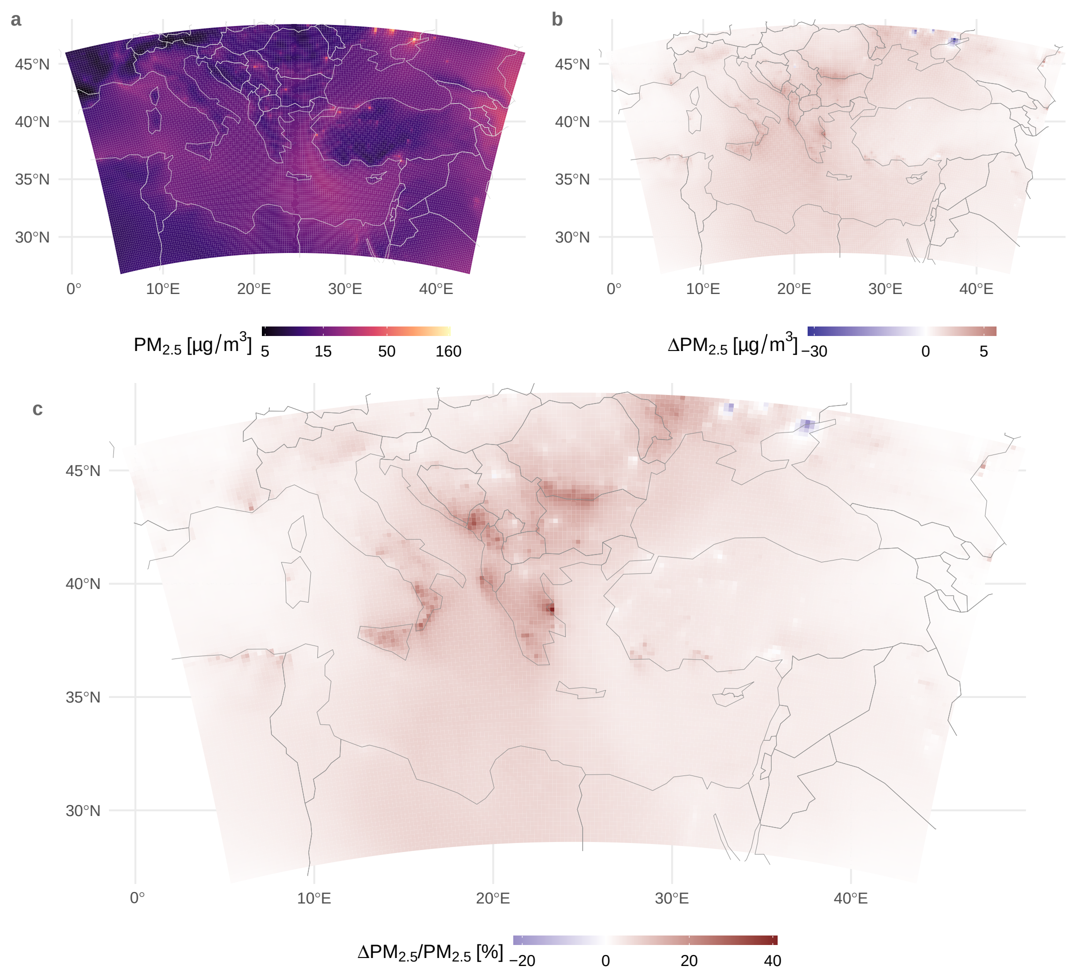

Figure 2. Spatial pattern of multi-month mean $PM_{2.5}$ concentrations simulated by WRF-Chem under the fires scenario and the difference relative to the no-fires scenario. a) $PM_{2.5}$ concentration simulated under fires scenario, b) $PM_{2.5}$ concentration under fires scenario relative to no-fires ($\Delta PM_{2.5}$ = ${PM_{2.5}}^{\text{fires}}$- ${PM_{2.5}}^{\text{no-fires}}$), c) $PM_{2.5}$ concentration attributable to wildfires in percentages ($\Delta PM_{2.5}/{PM_{2.5}}^{\text{fires}}$). The increased $PM_{2.5}$ concentrations caused by wildfires are mainly observed in the Balkans, Greece, and southern Italy, whereas the regions with high background industrial pollution (hot spots in the panel a) show a slight decrease in ambient $PM_{2.5}$ concentration.

Similar to $PM_{2.5}$, the diurnal pattern of NO_2 and SO_2 concentration is determined by the mixing layer height (Figure S10-S11 in SI). We do indeed find the expected increases in the concentration of the hydroxyl radical (OH) in the fire simulation (Figure S7 in SI), which will lead to additional formation of secondary particulate matter.

3.4 Population-weighted exposure to major air pollutants

Figure 4 depicts the multi-month mean population-weighted exposures to four air pollutants under fires (red dots), and no-fires (blue dots) scenarios. For the time series of population-weighted exposures to air pollutants in individual countries, please refer to Figures S12-S15. Countries in Balkans (e.g., Albania, North Macedonia, Montenegro, and Bulgaria), Romania, and Greece are among the most affected regions by the wildfire-

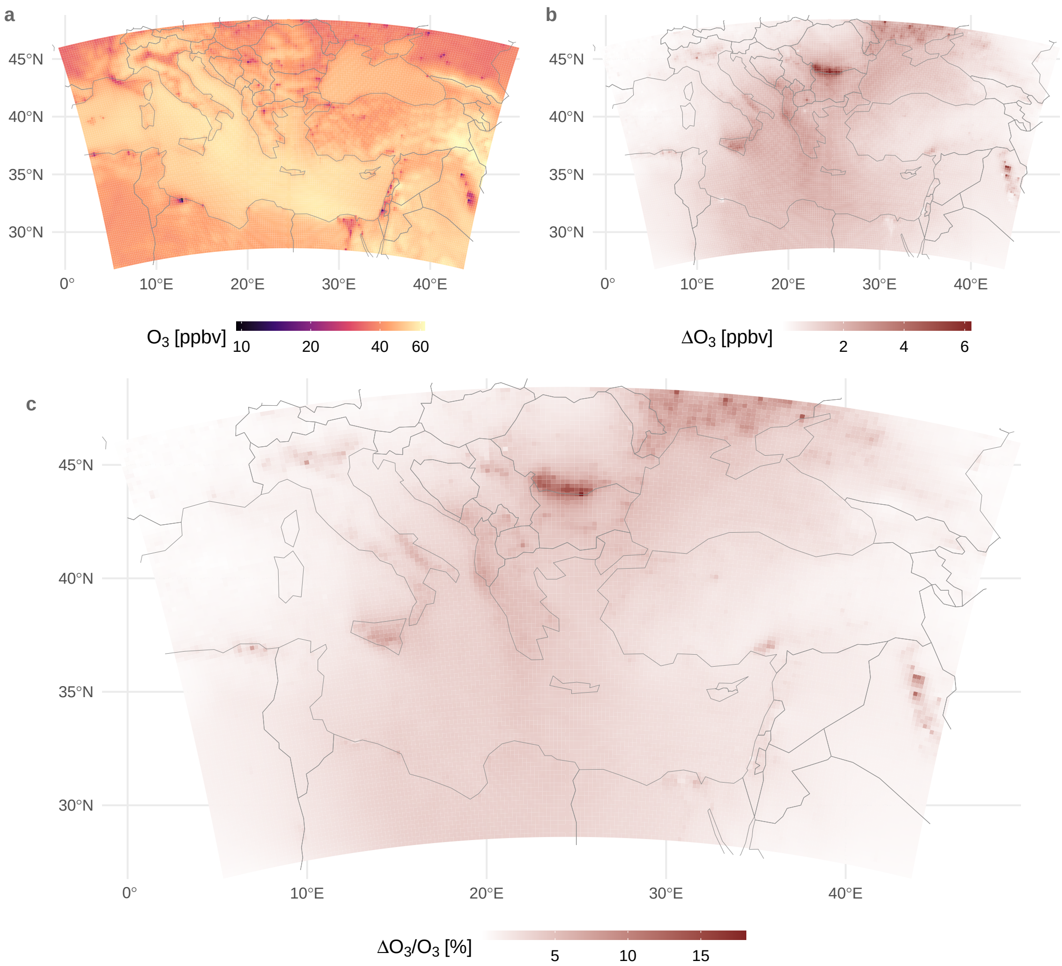

Figure 3. Spatial pattern of multi-month mean O_3 concentrations simulated by WRF-Chem under the fires scenario and the difference relative to the no-fires scenario. a) O_3 concentration simulated under fires scenario, b) O_3 concentration under fires scenario relative to no-fires ($\Delta O_3 = O_3^{\text{fires}}$- $O_3^{\text{no-fires}}$), c) O_3 concentration attributable to wildfires in percentages ($\Delta O_3/O_3^{\text{fires}}$).

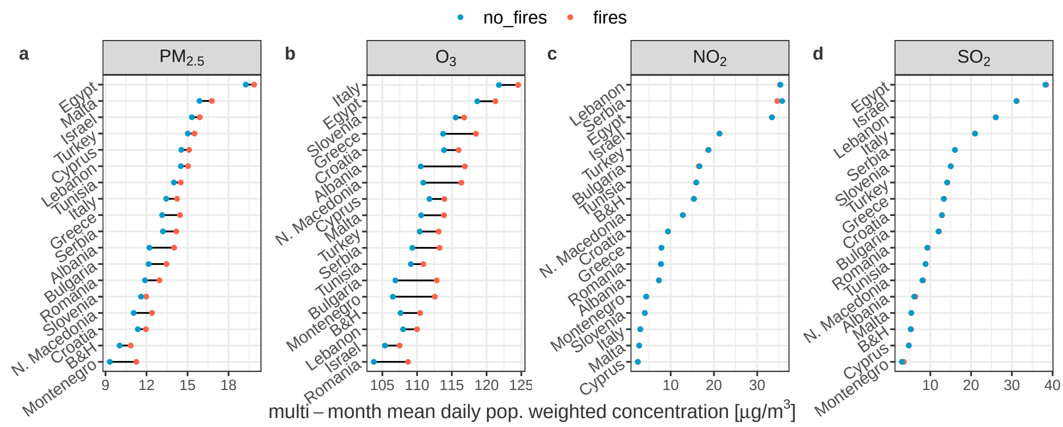

Figure 4. Multi-month daily mean population weighted concentration of air pollutants, fires scenario versus no-fires scenario. For pollutants other than O_3, the daily mean concentration is used, while the daily mean 8-h average (DMA8) for O_3. B&H stands for Bosnia and Herzegovina.

caused $PM_{2.5}$ and O_3 pollution, in line with the incidence of wildfires within the simulation period. By contrast, wildfires have not resulted in a discernible increase of population exposure to NO_2 and SO_2 within the simulation period and region. Therefore, we estimate the wildfire-associated health impacts based primarily on $PM_{2.5}$ and O_3 exposures.

3.5 Wildfire-caused excess mortality

Figure 5 a-b shows the excess number of deaths for each country estimated based separately on RRs of short-term exposure to $PM_{2.5}$ and O_3 obtained from the meta-analysis by Orellano et al. (2020). The 95% CIs are estimated using the Monte Carlo method described in Section 2.4.3. The exact number of deaths for each country and the entire region are available in Table S2 in SI.

Owing to the large population, Italy and Egypt are the countries with the highest excess death estimates due to short-term exposure to wildfire-caused $PM_{2.5}$ and O_3. Although wildfires are not frequently observed in Egypt (Figure 1 b), the deaths recorded are significant and can be attributed to the transport of air pollution caused by wildfires occurring elsewhere in the Mediterranean basin, clearly indicating the widespread impact of wildfires on the whole Mediterranean basin.

Figure 5 c-d sum up the excess deaths attributable to short-term exposure to $PM_{2.5}$ and O_3 in the entire region of investigation during mid-July to early October, 2021, based on RRs suggested by different publications. Based on the RR values from Orellano et al. (2020), there are 270 (95% CI: 177-370) deaths attributable to the short-term exposure to wildfire-caused $PM_{2.5}$. This estimate is close to the one based on Liu et al. (2019) – 281 (95%: 225-334). In comparison, 508 (95% CI: 187-847) excess deaths are estimated based on the RRs from World Health Organization (2013), albeit with a pronounced range of uncertainty.

With regard to the excess deaths attributable to short-term O_3 exposure, 741 (95% CI: 556 - 940]) excess deaths are estimated based on Orellano et al. (2020), remarkably exceeding the estimates based on World Health Organization (2013) (501, 95% 247-768) and Vicedo-Cabrera et al. (2020) (310, 95% 201-428).

4 Discussion and Conclusions

We have assessed the health impacts due to the short-term exposure to air pollution caused by wildfires over the eastern and central Mediterranean basin in the summer 2021. The exposures were estimated using a fully coupled atmospheric chemistry model under fire and no-fire scenarios, respectively, while the consequent health impacts were quantified based on well-established ERFs from selected systematic reviews. We estimated that the 2021 summer wildfires result in an excess number of deaths ranging from approximately 270 (95% CI: 177-370) to 741 (95% CI: 556 - 940]), depending on the targeted pollutants which population are exposed to, and on their respective ERFs.

In general, we found larger health impacts due to wildfire-associated exposure to O_3 than to $PM_{2.5}$. As the relative risk of exposure to O_3 is actually lower than that of $PM_{2.5}$ exposure (Table 1), the reason for this surprising finding is shown to be attributable to the more widespread impact of wildfires on O_3 due to a longer overall lifetime of O_3 in the atmosphere.

We refrained from deciding whether the excess deaths attributed to each pollutant can simply be added up to generate a synthesized estimate of health impacts as a result of the simultaneous exposure to multiple pollutants. The solution to this problem demands a thorough knowledge of correlations between health impacts of each pollutant (World Health Organization, 2013), and analysis of their confounding effects (Anderson

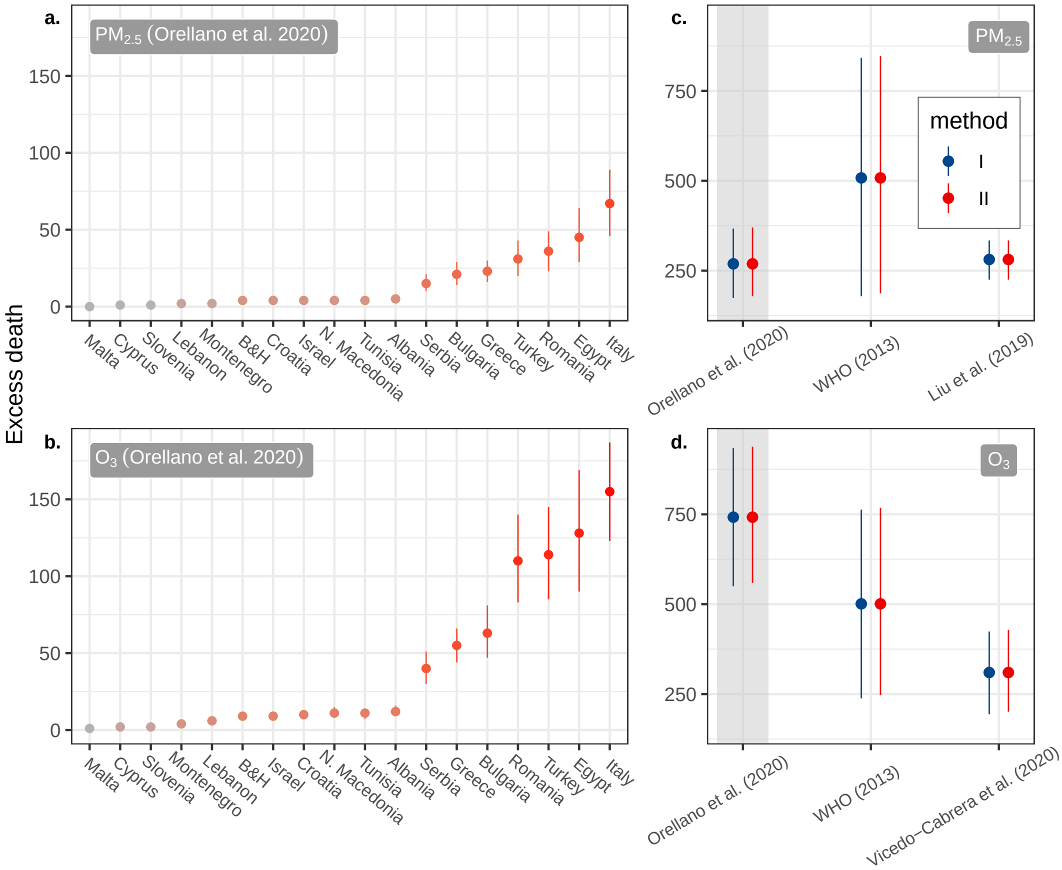

Figure 5. Excess deaths with uncertainties estimated based on relative risks of short-term exposure to $PM_{2.5}$ and O_3. a-b) wildfire-caused excess deaths with 95% CIs for each country included in the study based on relative risk values for short-term $PM_{2.5}$ and O_3 exposures from Orellano et al. (2020). c) Total excess deaths estimated using relative risk values from different meta-analyses (with the vertical gray band indicating the ones used in panels a and b), based on short-term exposure to $PM_{2.5}$ and O_3, respectively. The 95% CIs were estimated using the Delta (I) and Monte Carlo (II) methods. In Liu et al. (2019), the 2-day moving average of daily mean $PM_{2.5}$ concentrations was used to estimate the excess mortality.

et al., 2012; Bell et al., 2007). Although several statistical methods have been proposed to address the multi-collinearity issues in concurrent exposure (Stafoggia et al., 2017; Wei et al., 2020), they have not been widely adopted, including in studies that underlay the systematic reviews by Orellano et al. (2020); World Health Organization (2013). Therefore, results based on these reviews should be interpreted with caution, as confounders were not adequately adjusted for. As a result, it remains inconclusive whether to sum up the death estimates based on different air pollutants. All the aforementioned aspects can substantially affect the outcomes of the health impact assessment, making it difficult to narrow down the range of real health impacts attributable to wildfire-caused air pollution beyond what we have shown here.

The WRF-Chem model enables a temporally and spatially resolved exposure estimate, while accounting for primary emissions from wildfires and subsequent secondary chemical and physical processes. To date, the health impact assessment of air pollution is limited to a subset of its proxies (e.g., $PM_{2.5}$, NO_2, O_3), with their exposures being measured by mass. This simplification is increasingly challenged by mounting evidence that the toxicity of air pollution depends to a large extent on the chemical composition and atmospheric ageing rather than the mass itself. Especially, several studies point to the fact that particulate matter arising from wildfires is more toxic to lungs compared with particulate matter from normal ambient air (Wegesser et al., 2009; Dong et al., 2017; Xu et al., 2020). In the future, the ability of such modeling systems to estimate further harmful trace gases as well as chemically-speciated particulate matter may help overcome such limitations, leading to better association and causation in epidemiological analysis.

We have accounted for uncertainties arose from the baseline mortality data and ERFs. However, we have to acknowledge several sources of uncertainty that have not been taken into account within this study. The health impacts estimated within the study is limited to the excess mortality due to short-term exposure to air pollution aggravated by wildfires. This does not take into account direct loss of life and hospital admissions caused by the direct exposure to radiant heat/smoke/flames of wildfires, nor the consequent impairment of life quality.

Though broadly validated, the WRF-Chem model results contain a certain degree of uncertainty in exposure estimation. The uncertainty could originate from the model configuration (e.g., the horizontal and vertical grid setting of simulation domain, and parameterization schemes adopted to account for the atmospheric physics and chemistry), model inputs (e.g., boundary meteorology, and inventories on anthropogenic and fires-associated emissions), as well as the representation of particles and their size distribution within the model (Im et al., 2018).

The horizontal resolution of 20 km set in the WRF-Chem simulation may be too coarse to represent urban areas and their related impacts on the dispersion and transformation of air pollutants sourced from wildfires. This may lead to an underestimation of particular matter and an overestimation of O_3 in urban areas (Im et al., 2015a). Due to its complex nature, the model-associated uncertainty has not been addressed in the study. However, this can be the focus of future research.

A further source of uncertainty lies in the ERFs adopted for the health impact assessment. Although ERFs derived from meta-analysis are thought to deliver less biased and impartial evidence on the association between exposure and health outcomes, they are prone to several other biases, e.g., publication bias and language bias, which may distort the evidence (Page et al., 2021). Meanwhile, current ERFs are based primarily on exposures measured in urban or suburban settings, making the exposure estimate for rural areas more prone to misclassification errors. Even though rural areas normally exhibit a lower level of particulate matters and are thought to be less polluted, the rural air can demonstrate similar levels of cellular oxidative potential as in cities, due largely to more toxic chemicals emitted from agriculture activities (Wang et al., 2022). On the other hand, neither measurements by monitoring networks nor model simulations, are able to reproduce the individual exposure which is subject to a variety of factors such as personal behavior, socioeconomic status, and preexisting health conditions (Evangelopoulos et al., 2020).

Regarding the large differences in estimated health impacts for O_3, we note that, as a systematic review commissioned by the WHO, Orellano et al. (2020) included the most recent studies, providing updated evidence base supporting associations between short-term air pollution exposure and mortality, compared to World Health Organization (2013). In contrast, Vicedo-Cabrera et al. (2020) suggested a considerably lower RR for short-term exposure to O_3, resulting in a smaller estimate of excess deaths. As both studies differ in methodology and underlying database leading to the relative risks, the reason for the discrepancy remains unexplored and is beyond the scope of this study.

In all estimates, the choice of methods for quantifying the uncertainty of excess deaths exhibits a minor impact on the results. The Delta method, compared with the Monte Carlo method, is prone to slightly underestimate the lower and upper bounds of the 95% CI.

We excluded the health impact assessment based on short-term exposure to PM_{10}, another widely used proxy indicator for air pollution, to avoid double counting of the PM-associated health effects. This is based on the fact that $PM_{2.5}$ accounts for an overwhelming proportion of PM-associated health effects (Lu et al., 2015; Liu et al., 2019).

Future work is needed to reduce the uncertainties resulted from estimates of both exposures and health effects, while simultaneously augmenting the computational performance of the methodology used. To this end, it is worth further exploring the ensemble or hybrid approaches which combine both physically based atmospheric chemistry transport models and computationally efficient statistical models (Im et al., 2018; Conibear et al., 2021; Di et al., 2019; Shtein et al., 2019; Hough et al., 2021).

Conflict of Interest

The authors declare no conflict of interest.

Data Availability Statement

Data sets supporting the findings of this study are publicly available. GPW v4 population count data from the Center for International Earth Science Information Network (CIESIN) are available via `https://doi.org/10.7927/H4PN93PB`. All-age all-cause both-gender mortality data for the countries included in the study are available via he Global Health Data Exchange (GHDx), downloaded from `https://ghdx.healthdata.org/gbd-results-tool?params=gbd-api-2019-permalink/4e1860d6fad20ccf64c5e6f7e1f7a24b`. Monthly base-line mortality data (2010-2019) for the member and associated states of European Statistical Office (Eurostat) are available via `https://ec.europa.eu/eurostat/databrowser/view/DEMO_MMONTH/default/table?lang=en&category=demo.demo_mor`. European Environmental Agency (EEA)'s AirBase air quality time series data sets (E1a & E2a) were downloaded using `airbase 0.2.7` python library (`https://pypi.org/project/airbase/`). Most data processing, analyses, and visualization were performed using R software (version 4.1.1) (R Core Team, 2021). R codes and essential WRF-Chem simulation results leading to the results of this study are currently (upon submission) stored in an internal repository hosted by the University of Augsburg. They will be shared via a public repository during the review process.

Acknowledgments

The authors acknowledge the European Forest Fire Information System of the European Commission for providing the data on total number of wildfires and total area of burnt areas. We acknowledge use of the WRF-Chem preprocessor tools mozbc, bio_emiss, fire_emiss and anthro_emiss provided by the Atmospheric Chemistry Observations and Modeling Lab (ACOM) of NCAR. The authors gratefully acknowledge computing time at the Augsburg Linux Compute Cluster (ALCC). Additional thanks go to David Jean du Preez for proofreading this paper.

References

Anderson, G. B., Krall, J. R., Peng, R. D., & Bell, M. L. (2012). Is the relation between ozone and mortality confounded by chemical components of particulate matter? Analysis of 7 components in 57 US communities. *American Journal of Epidemiology*, *176*(8), 726–732. doi: 10.1093/aje/kws188

Anenberg, S. C., Horowitz, L. W., Tong, D. Q., & West, J. J. (2010). An estimate of the global burden of anthropogenic ozone and fine particulate matter on premature human mortality using atmospheric modeling. *Environmental Health Perspectives*, *118*(9), 1189–1195. doi: 10.1289/ehp.0901220

Bell, M. L., Kim, J. Y., & Dominici, F. (2007). Potential confounding of particulate matter on the short-term association between ozone and mortality in multisite time-series studies. *Environmental Health Perspectives*, *115*(11), 1591–1595. doi: 10.1289/ehp.10108

Bencherif, H., Bègue, N., Pinheiro, D. K., du Preez, D. J., Cadet, J. M., Lopes, F. J. d. S., ... Clerbaux, C. (2020). Investigating the long-range transport of aerosol plumes following the amazon fires (August 2019): A multi-instrumental approach from ground-based and satellite observations. *Remote Sensing*, *12*(22), 1–18. doi: 10.3390/rs12223846

Bowman, D. M. J. S., Kolden, C. A., Abatzoglou, J. T., Johnston, F. H., van der Werf, G. R., & Flannigan, M. (2020, oct). Vegetation fires in the Anthropocene. *Nature Reviews Earth & Environment*, *1*(10), 500–515. doi: 10.1038/s43017-020-0085-3

Brunekreef, B., & Holgate, S. T. (2002). Air pollution and health. *Lancet*, *360*(9341), 1233–1242. doi: 10.1016/S0140-6736(02)11274-8

Burke, M., Driscoll, A., Heft-Neal, S., Xue, J., Burney, J., & Wara, M. (2021). The changing risk and burden of wildfire in the United States. *Proceedings of the National Academy of Sciences of the United States of America*, *118*(2), 1–6. doi: 10.1073/PNAS.2011048118

Burnett, R. T., Arden Pope, C., Ezzati, M., Olives, C., Lim, S. S., Mehta, S., ... Cohen, A. (2014). An integrated risk function for estimating the global burden of disease attributable to ambient fine particulate matter exposure. *Environmental Health Perspectives*, *122*(4), 397–403. doi: 10.1289/ehp.1307049

Butt, E. W., Conibear, L., Knote, C., & Spracklen, D. V. (2021, jul). Large Air Quality and Public Health Impacts due to Amazonian Deforestation Fires in 2019. *GeoHealth*, *5*(7), 1–16. doi: 10.1029/2021GH000429

CAMS. (2021). *Wildfires wreaked havoc in 2021, CAMS tracked their impact.* Retrieved from `https://atmosphere.copernicus.eu/wildfires-wreaked-havoc-2021-cams-tracked-their-impact(Accessed:2022-02-01)`

Chen, G., Guo, Y., Yue, X., Tong, S., Gasparrini, A., Bell, M. L., ... Li, S. (2021, sep). Mortality risk attributable to wildfire-related PM2·5 pollution: a global time series study in 749 locations. *The Lancet Planetary Health*, *5*(9), e579–e587. doi: 10.1016/S2542-5196(21)00200-X

CIESIN. (2018). *Gridded Population of the World, Version 4 (GPWv4): Population Count Adjusted to Match 2015 Revision of UN WPP Country Totals, Revi-*

sion 11. Palisades, NY: NASA Socioeconomic Data and Applications Center (SEDAC). Retrieved from `https://doi.org/10.7927/H4PN93PB`

Cohen, A. J., Brauer, M., Burnett, R., Anderson, H. R., Frostad, J., Estep, K., ... Forouzanfar, M. H. (2017). Estimates and 25-year trends of the global burden of disease attributable to ambient air pollution: an analysis of data from the Global Burden of Diseases Study 2015. *The Lancet*, *389*(10082), 1907–1918. doi: 10.1016/S0140-6736(17)30505-6

Conibear, L., Reddington, C. L., Silver, B. J., Chen, Y., Knote, C., Arnold, S. R., & Spracklen, D. V. (2021). Statistical Emulation of Winter Ambient Fine Particulate Matter Concentrations From Emission Changes in China. *GeoHealth*, *5*(5), 1–13. doi: 10.1029/2021GH000391

Cos, J., Doblas-Reyes, F., Jury, M., Marcos, R., Bretonnière, P.-A., & Samsó, M. (2021). The Mediterranean climate change hotspot in the CMIP5 and CMIP6 projections. *Earth System Dynamics Discussions*(2018), 1–26. doi: 10.5194/esd-2021-65

Di, Q., Amini, H., Shi, L., Kloog, I., Silvern, R., Kelly, J., ... Schwartz, J. (2019, sep). An ensemble-based model of PM2.5 concentration across the contiguous United States with high spatiotemporal resolution. *Environment International*, *130*(July), 104909. doi: 10.1016/j.envint.2019.104909

Dong, T. T., Hinwood, A. L., Callan, A. C., Zosky, G., & Stock, W. D. (2017). In vitro assessment of the toxicity of bushfire emissions: A review. *Science of the Total Environment*, *603-604*, 268–278. doi: 10.1016/j.scitotenv.2017.06.062

EFFIS. (2021). *Total burnt areas and total number of fires in 2021.* Author. Retrieved from `https://effis.jrc.ec.europa.eu/applications/data-and-services(accessed:2021-12-01)`

Emmons, L. K., Walters, S., Hess, P. G., Lamarque, J.-F., Pfister, G. G., Fillmore, D., ... Kloster, S. (2010). Description and evaluation of the model for ozone and related chemical tracers, version 4 (mozart-4). *Geoscientific Model Development*, *3*(1), 43–67. doi: 10.5194/gmd-3-43-2010

European Environment Agency. (2021). *AirBase air quality data (E1a & E2a).* Retrieved from `https://discomap.eea.europa.eu/map/fme/AirQualityExport.htm`

Eurostat. (2021). *Deaths (total) by month, 2010-2019.* Luxembourg.

Evangelopoulos, D., Katsouyanni, K., Keogh, R. H., Samoli, E., Schwartz, J., Barratt, B., ... Walton, H. (2020, apr). PM2.5 and NO2 exposure errors using proxy measures, including derived personal exposure from outdoor sources: A systematic review and meta-analysis. *Environment International*, *137*(2), 105500. doi: 10.1016/j.envint.2020.105500

Global Burden of Disease Collaborative Network. (2020). *Global Burden of Disease Study 2019 (GBD 2019) Results.* Seattle, United States: Institute for Health Metrics and Evaluation (IHME). Retrieved from `http://ghdx.healthdata.org/gbd-results-tool?params=gbd-api-2019-permalink/4e1860d6fad20ccf64c5e6f7e1f7a24b`

Gong, S. (2003). A parameterization of sea-salt aerosol source function for sub-and super-micron particles. *Global biogeochemical cycles*, *17*(4).

Graham, A. M., Pringle, K. J., Pope, R. J., Arnold, S. R., Conibear, L. A., Burns, H., ... McQuaid, J. B. (2021, oct). Impact of the 2019/2020 Australian Megafires on Air Quality and Health. *GeoHealth*, *5*(10), 1–17. doi: 10.1029/2021GH000454

Grell, G. A., Peckham, S. E., Schmitz, R., McKeen, S. A., Frost, G., Skamarock, W. C., & Eder, B. (2005). Fully coupled "online" chemistry within the wrf model. *Atmospheric Environment*, *39*(37), 6957–6975.

Guenther, A., Karl, T., Harley, P., Wiedinmyer, C., Palmer, P. I., & Geron, C. (2006). Estimates of global terrestrial isoprene emissions using megan (model of emissions of gases and aerosols from nature). *Atmospheric Chemistry and*

Physics, *6*(11), 3181–3210.
Haikerwal, A., Akram, M., Monaco, A. D., Smith, K., Sim, M. R., Meyer, M., ... Dennekamp, M. (2015). Impact of fine particulate matter (PM2.5) exposure during wildfires on cardiovascular health outcomes. *Journal of the American Heart Association*, *4*(7), 1–10. doi: 10.1161/JAHA.114.001653
Hodzic, A., & Jimenez, J. L. (2011). Modeling anthropogenically controlled secondary organic aerosols in a megacity: a simplified framework for global and climate models. *Geoscientific Model Development*, *4*(4), 901–917. doi: 10.5194/gmd-4-901-2011
Hough, I., Sarafian, R., Shtein, A., Zhou, B., Lepeule, J., & Kloog, I. (2021). Gaussian Markov random fields improve ensemble predictions of daily 1 km PM2.5 and PM10 across France. *Atmospheric Environment*, *264*(May), 118693. Retrieved from `https://doi.org/10.1016/j.atmosenv.2021.118693` doi: 10.1016/j.atmosenv.2021.118693
Im, U., Bianconi, R., Solazzo, E., Kioutsioukis, I., Badia, A., Balzarini, A., ... Galmarini, S. (2015a). Evaluation of operational online-coupled regional air quality models over Europe and North America in the context of AQMEII phase 2. Part II: Particulate matter. *Atmospheric Environment*, *115*, 421–441. doi: 10.1016/j.atmosenv.2014.08.072
Im, U., Bianconi, R., Solazzo, E., Kioutsioukis, I., Badia, A., Balzarini, A., ... Galmarini, S. (2015b). Evaluation of operational on-line-coupled regional air quality models over Europe and North America in the context of AQMEII phase 2. Part I: Ozone. *Atmospheric Environment*, *115*, 404–420. doi: 10.1016/j.atmosenv.2014.09.042
Im, U., Brandt, J., Geels, C., Hansen, K. M., Christensen, J. H., Andersen, M. S., ... Galmarini, S. (2018, apr). Assessment and economic valuation of air pollution impacts on human health over Europe and the United States as calculated by a multi-model ensemble in the framework of AQMEII3. *Atmospheric Chemistry and Physics*, *18*(8), 5967–5989. doi: 10.5194/acp-18-5967-2018
Jaffe, D. A., & Wigder, N. L. (2012). Ozone production from wildfires: A critical review. *Atmospheric Environment*, *51*, 1–10. Retrieved from `http://dx.doi.org/10.1016/j.atmosenv.2011.11.063` doi: 10.1016/j.atmosenv.2011.11.063
Janssens-Maenhout, G., Dentener, F., Aardenne, J. V., Monni, S., Pagliari, V., Orlandini, L., ... Keating, T. (2012). *EDGAR-HTAP: a harmonized gridded air pollution emission dataset based on national inventories.* Retrieved from `https://edgar.jrc.ec.europa.eu/dataset_htap_v1` doi: 10.2788/14102
Johnston, F. H., Henderson, S. B., Chen, Y., Randerson, J. T., Marlier, M., DeFries, R. S., ... Brauer, M. (2012, may). Estimated Global Mortality Attributable to Smoke from Landscape Fires. *Environmental Health Perspectives*, *120*(5), 695–701. doi: 10.1289/ehp.1104422
Jolly, W. M., Cochrane, M. A., Freeborn, P. H., Holden, Z. A., Brown, T. J., Williamson, G. J., & Bowman, D. M. (2015). Climate-induced variations in global wildfire danger from 1979 to 2013. *Nature Communications*, *6*(May), 1–11. doi: 10.1038/ncomms8537
Knote, C., Hodzic, A., Jimenez, J. L., Volkamer, R., Orlando, J. J., Baidar, S., ... Zhang, Q. (2014). Simulation of semi-explicit mechanisms of soa formation from glyoxal in aerosol in a 3-d model. *Atmospheric Chemistry and Physics*, *14*(12), 6213–6239. doi: 10.5194/acp-14-6213-2014
Kramer, H. A., Mockrin, M. H., Alexandre, P. M., & Radeloff, V. C. (2019). High wildfire damage in interface communities in California. *International Journal of Wildland Fire*, *28*(9), 641–650. doi: 10.1071/WF18108
Kroll, J. H., Heald, C. L., Cappa, C. D., Farmer, D. K., Fry, J. L., Murphy, J. G., & Steiner, A. L. (2020). The complex chemical effects of COVID-19 shutdowns on air quality. *Nature Chemistry*, *12*(9), 777–779. doi:

10.1038/s41557-020-0535-z
LeGrand, S. L., Polashenski, C., Letcher, T. W., Creighton, G. A., Peckham, S. E., & Cetola, J. D. (2019). The afwa dust emission scheme for the gocart aerosol model in wrf-chem v3. 8.1. *Geoscientific Model Development*, *12*(1), 131–166.
Lelieveld, J., Pozzer, A., Pöschl, U., Fnais, M., Haines, A., & Münzel, T. (2020). Loss of life expectancy from air pollution compared to other risk factors: A worldwide perspective. *Cardiovascular Research*, *116*(11), 1910–1917. doi: 10.1093/cvr/cvaa025
Linares, C., Díaz, J., Negev, M., Martínez, G. S., Debono, R., & Paz, S. (2020). Impacts of climate change on the public health of the Mediterranean Basin population - Current situation, projections, preparedness and adaptation. *Environmental Research*, *182*(January), 109107. doi: 10.1016/j.envres.2019.109107
Liu, C., Chen, R., Sera, F., Vicedo-Cabrera, A. M., Guo, Y. Y.-L., Tong, S., ... Kan, H. (2019). Ambient Particulate Air Pollution and Daily Mortality in 652 Cities. *New England Journal of Medicine*, *381*(8), 705–715. doi: 10.1056/nejmoa1817364
Lu, F., Xu, D., Cheng, Y., Dong, S., Guo, C., Jiang, X., & Zheng, X. (2015). Systematic review and meta-analysis of the adverse health effects of ambient PM2.5 and PM10 pollution in the Chinese population. *Environmental Research*, *136*, 196–204. doi: 10.1016/j.envres.2014.06.029
Macintyre, H. L., Heaviside, C., Neal, L. S., Agnew, P., Thornes, J., & Vardoulakis, S. (2016). Mortality and emergency hospitalizations associated with atmospheric particulate matter episodes across the UK in spring 2014. *Environment International*, *97*, 108–116. doi: 10.1016/j.envint.2016.07.018
Manning, M. I., Martin, R. V., Hasenkopf, C., Flasher, J., & Li, C. (2018). Diurnal Patterns in Global Fine Particulate Matter Concentration. *Environmental Science and Technology Letters*, *5*(11), 687–691. doi: 10.1021/acs.estlett.8b00573
Mansournia, M. A., & Altman, D. G. (2018). Population attributable fraction. *BMJ (Online)*, *360*(February), 2–3. doi: 10.1136/bmj.k757
Naeher, L. P., Brauer, M., Lipsett, M., Zelikoff, J. T., Simpson, C. D., Koenig, J. Q., & Smith, K. R. (2007). Woodsmoke health effects: A review. *Inhalation Toxicology*, *19*(1), 67–106. doi: 10.1080/08958370600985875
Orellano, P., Reynoso, J., Quaranta, N., Bardach, A., & Ciapponi, A. (2020). Short-term exposure to particulate matter (PM10 and PM2.5), nitrogen dioxide (NO2), and ozone (O3) and all-cause and cause-specific mortality: Systematic review and meta-analysis. *Environment International*, *142*(December 2019), 105876. doi: 10.1016/j.envint.2020.105876
Page, M. J., Sterne, J. A. C., Higgins, J. P. T., & Egger, M. (2021, mar). Investigating and dealing with publication bias and other reporting biases in meta-analyses of health research: A review. *Research Synthesis Methods*, *12*(2), 248–259. doi: 10.1002/jrsm.1468
Pebesma, E. (2018). Simple Features for R: Standardized Support for Spatial Vector Data. *The R Journal*, *10*(1), 439–446. doi: 10.32614/RJ-2018-009
R Core Team. (2021). R: A language and environment for statistical computing [Computer software manual]. Vienna, Austria. Retrieved from `https://www.R-project.org/`
Ruffault, J., Curt, T., Moron, V., Trigo, R. M., Mouillot, F., Koutsias, N., ... Belhadj-Khedher, C. (2020). Increased likelihood of heat-induced large wildfires in the Mediterranean Basin. *Scientific Reports*, *10*(1), 1–9. doi: 10.1038/s41598-020-70069-z
Rutledge, G. K., Alpert, J., & Ebisuzaki, W. (2006). NOMADS: A climate and weather model archive at the National Oceanic and Atmospheric Administration. *Bulletin of the American Meteorological Society*, *87*(3), 327–341. Retrieved from `https://nomads.ncep.noaa.gov` doi: 10.1175/BAMS-87-3-327

Schneider, S. R., & Abbatt, J. P. (2022). Wildfire atmospheric chemistry: climate and air quality impacts. *Trends in Chemistry*, *4*(4), 255-257. (Special Issue: Third Anniversary) doi: https://doi.org/10.1016/j.trechm.2021.12.004

Schwarz, L., Dimitrova, A., Aguilera, R., Basu, R., Gershunov, A., & Benmarhnia, T. (2022). Smoke and COVID-19 case fatality ratios during California wildfires. *Environmental Research Letters*, *17*(1), 014054. doi: 10.1088/1748-9326/ac4538

Shtein, A., Kloog, I., Schwartz, J., Silibello, C., Michelozzi, P., Gariazzo, C., ... Stafoggia, M. (2019). Estimating daily PM2.5 and PM10 over Italy using an ensemble model. *Environmental Science and Technology*, *54*, acs.est.9b04279. doi: 10.1021/acs.est.9b04279

Stafoggia, M., Breitner, S., Hampel, R., & Basagaña, X. (2017). Statistical Approaches to Address Multi-Pollutant Mixtures and Multiple Exposures: the State of the Science. *Current environmental health reports*, *4*(4), 481–490. doi: 10.1007/s40572-017-0162-z

Ver Hoef, J. M. (2012). Who invented the delta method? *American Statistician*, *66*(2), 124–127. doi: 10.1080/00031305.2012.687494

Vicedo-Cabrera, A. M., Sera, F., Liu, C., Armstrong, B., Milojevic, A., Guo, Y. Y. L. L., ... Gasparrini, A. (2020). Short term association between ozone and mortality: global two stage time series study in 406 locations in 20 countries. *The BMJ*, *368*, 1–10. doi: 10.1136/bmj.m108

Wang, Y., Puthussery, J. V., Yu, H., Liu, Y., Salana, S., & Verma, V. (2022). Sources of cellular oxidative potential of water-soluble fine ambient particulate matter in the Midwestern United States. *Journal of Hazardous Materials*, *425*(September 2021), 127777. doi: 10.1016/j.jhazmat.2021.127777

Wegesser, T. C., Pinkerton, K. E., & Last, J. A. (2009). California wildfires of 2008: Coarse and fine particulate matter toxicity. *Environmental Health Perspectives*, *117*(6), 893–897. doi: 10.1289/ehp.0800166

Wei, Y., Wang, Y., Wu, X., Di, Q., Shi, L., Koutrakis, P., ... Schwartz, J. D. (2020). Causal effects of air pollution on mortality rate in Massachusetts. *American Journal of Epidemiology*, *189*(11), 1316–1323. doi: 10.1093/aje/kwaa098

WHO. (2016). Health Risk Assessment of air pollution. *World Health Organization*, 1–40.

WHO. (2021). *WHO global air quality guidelines. Particulate matter (PM2.5 and PM10), ozone, nitrogen dioxide, sulfur dioxide and carbon monoxide.*

Wiedinmyer, C., Akagi, S., Yokelson, R. J., Emmons, L., Al-Saadi, J., Orlando, J., & Soja, A. (2011). The fire inventory from ncar (finn): A high resolution global model to estimate the emissions from open burning. *Geoscientific Model Development*, *4*(3), 625–641.

World Bank. (2020). *Total population.* The World Bank Group. Retrieved from `https://data.worldbank.org/indicator/SP.POP.TOTL(Accessed11Dec.2021)`

World Health Organization. (2013). Health risks of air pollution in Europe – HRAPIE project. *World Heath Organization (WHO)*, 60.

Xie, Y., Lin, M., & Horowitz, L. W. (2020). Summer PM2.5 Pollution Extremes Caused by Wildfires Over the Western United States During 2017–2018. *Geophysical Research Letters*, *47*(16), 1–11. doi: 10.1029/2020GL089429

Xu, R., Yu, P., Abramson, M. J., Johnston, F. H., Samet, J. M., Bell, M. L., ... Guo, Y. (2020, nov). Wildfires, Global Climate Change, and Human Health. *New England Journal of Medicine*, *383*(22), 2173–2181. doi: 10.1056/NEJMsr2028985

Zaveri, R. A., Easter, R. C., Fast, J. D., & Peters, L. K. (2008). Model for simulating aerosol interactions and chemistry (mosaic). *Journal of Geophysical Research: Atmospheres*, *113*(D13).

Zhou, X., Josey, K., Kamareddine, L., Caine, M. C., Liu, T., Mickley, L. J., ... Dominici, F. (2021). Excess of COVID-19 cases and deaths due to fine particulate matter exposure during the 2020 wildfires in the United States. *Science Advances*, *7*(33), 1–12. doi: 10.1126/sciadv.abi8789

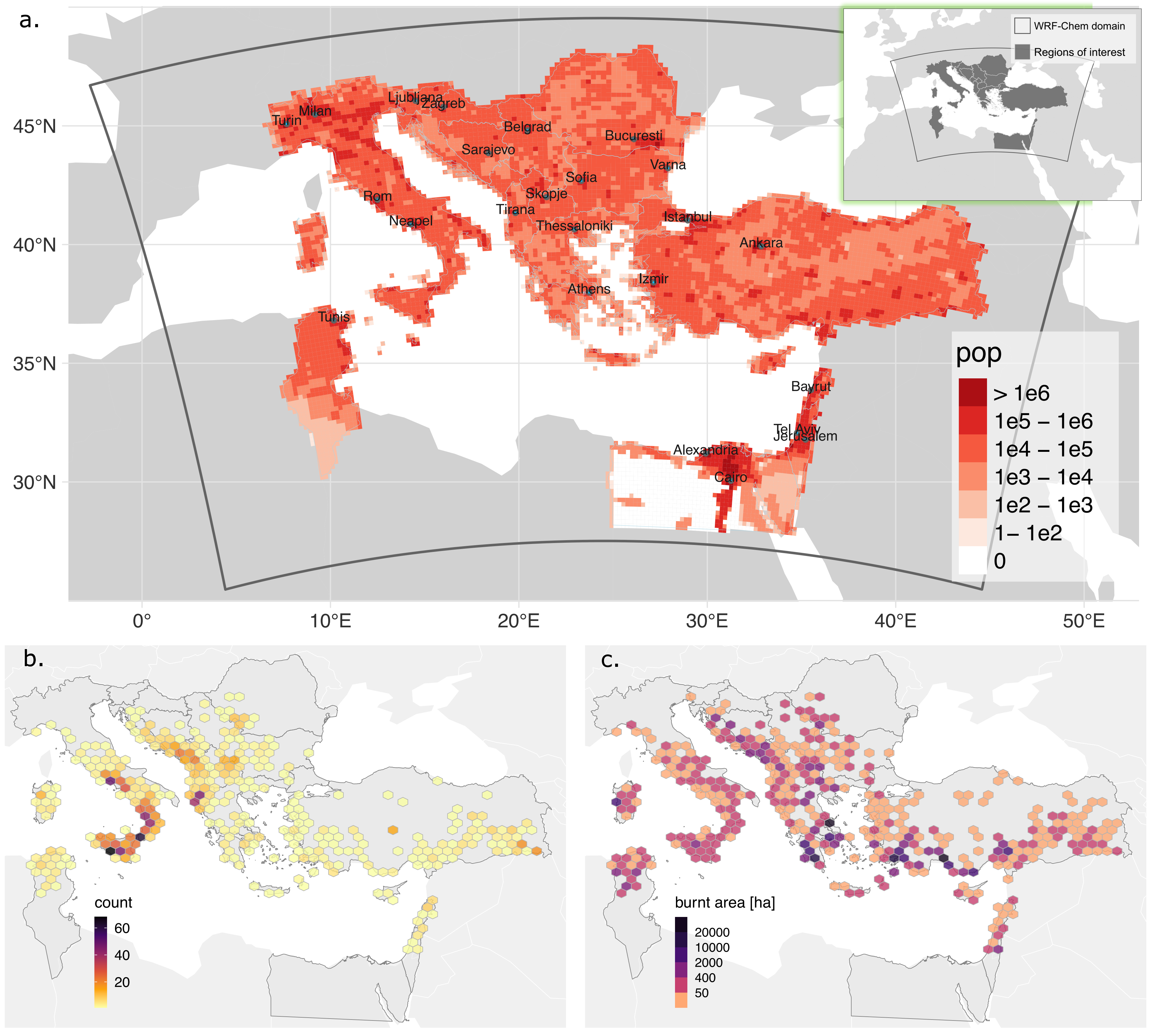

a.
WRF-Chem domain
Regions of interest
Turin
Milan
Ljubljana
Zagreb
Belgrad
Bucuresti
Sarajevo
Varna
Sofia
Skopje
Rom
Tirana
Neapel
Istanbul
Thessaloniki
Ankara
Izmir
Athens
Tunis
Bayrut
Tel Aviv
Jerusalem
Alexandria
Cairo
pop
> 1e6
1e5 – 1e6
1e4 – 1e5
1e3 – 1e4
1e2 – 1e3
1– 1e2
0
45°N
40°N
35°N
30°N
0°
10°E
20°E
30°E
40°E
50°E
b.
count
60
40
20
c.
burnt area [ha]
20000
10000
2000
400
50

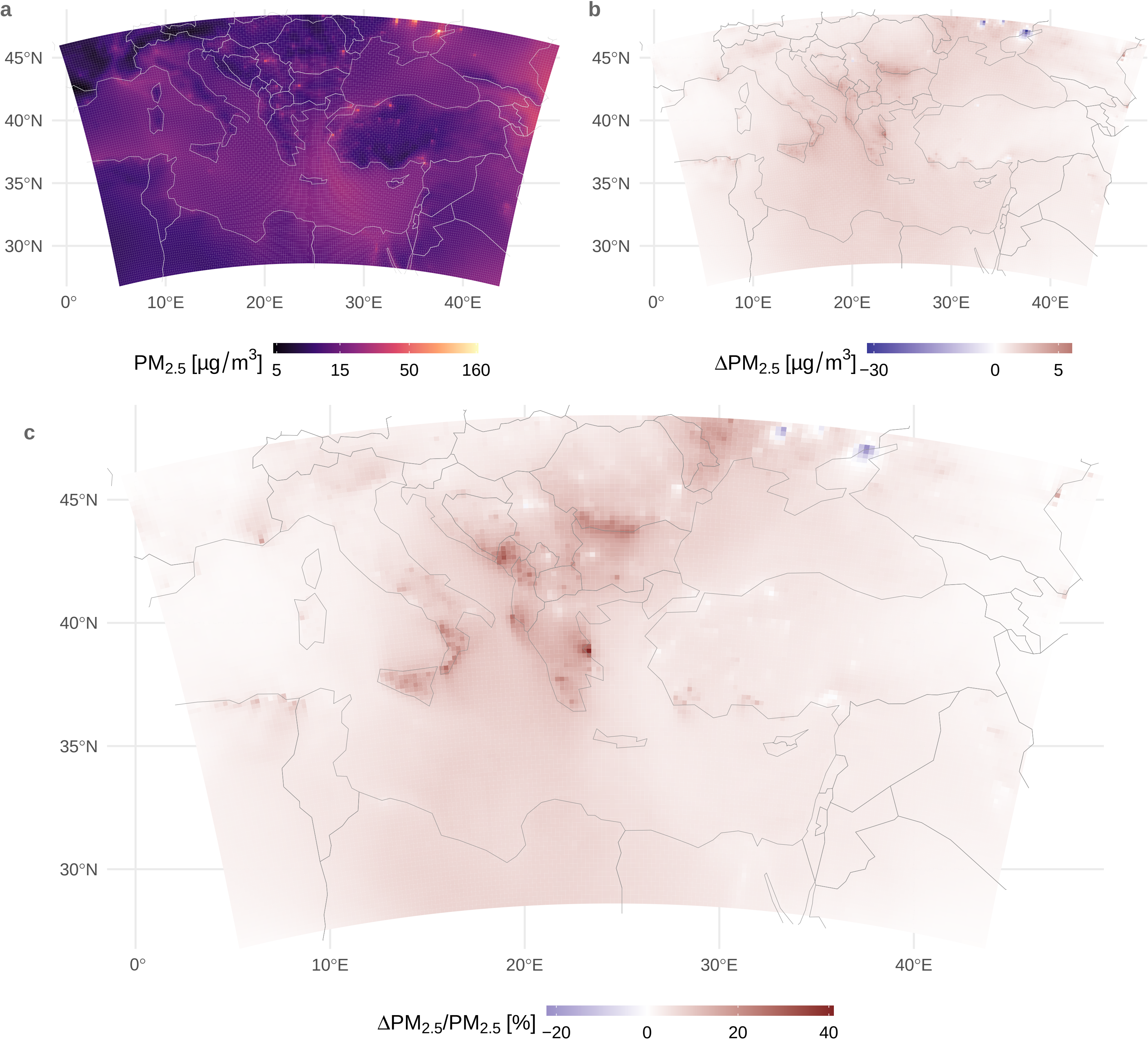
a
b
c
45°N
40°N
35°N
30°N
0°
10°E
20°E
30°E
40°E
PM2.5 [μg/m3]
5
15
50
160
ΔPM2.5 [μg/m3]
−30
0
5
ΔPM2.5/PM2.5 [%]
−20
0
20
40

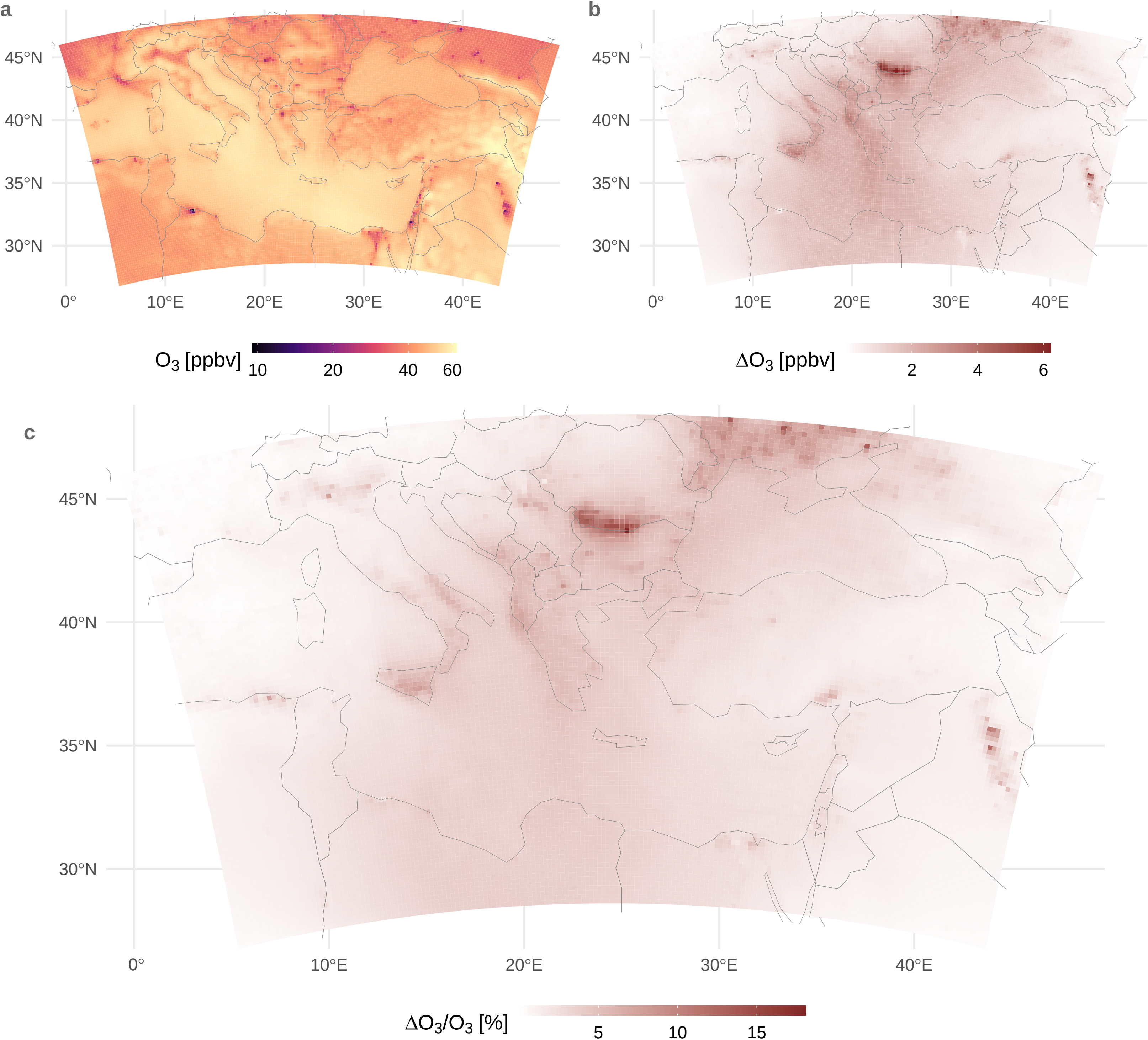

a
45°N
40°N
35°N
30°N
0°
10°E
20°E
30°E
40°E
O3 [ppbv]
10
20
40
60
b
ΔO3 [ppbv]
2
4
6
c
5
10
15
ΔO3/O3 [%]

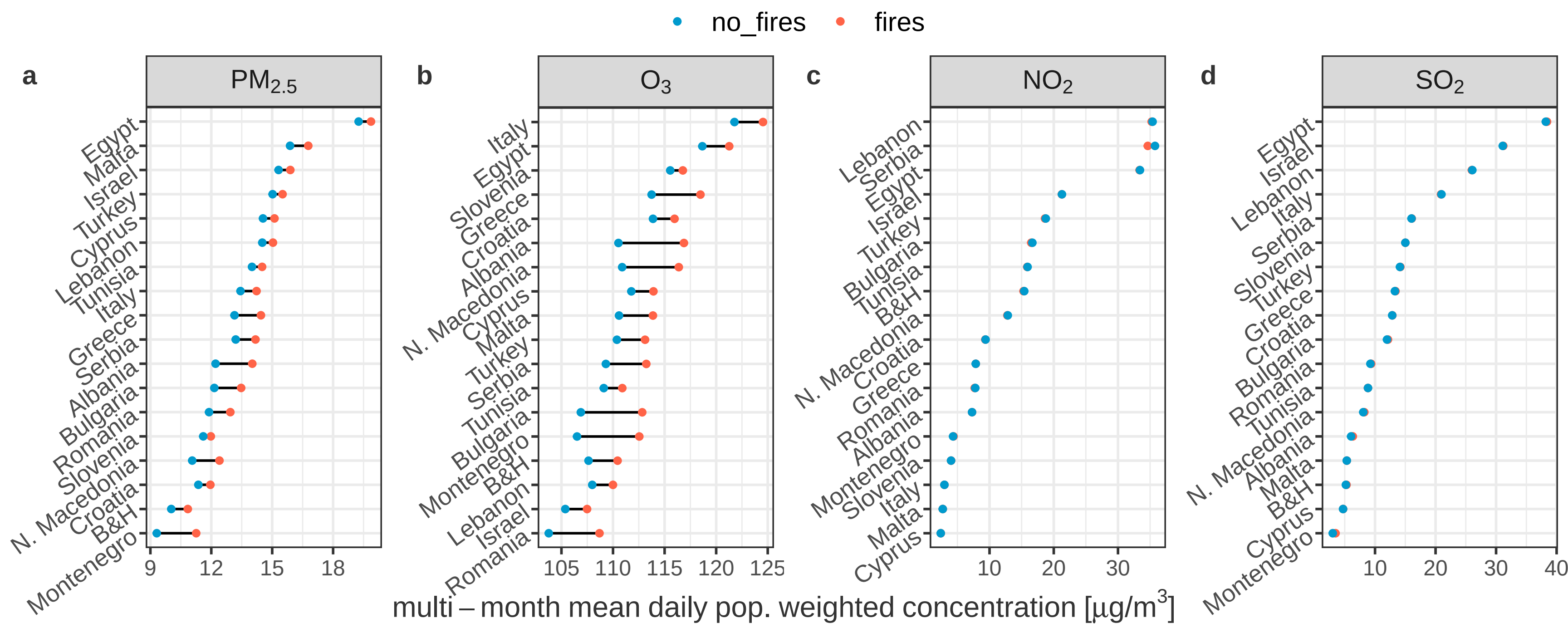

no_fires
fires
a
PM2.5
b
O3
c
NO2
d
SO2
Egypt
Malta
Israel
Turkey
Cyprus
Lebanon
Tunisia
Italy
Greece
Serbia
Albania
Bulgaria
Romania
Slovenia
N. Macedonia
Croatia
B&H
Montenegro
multi – month mean daily pop. weighted concentration [μg/m3]

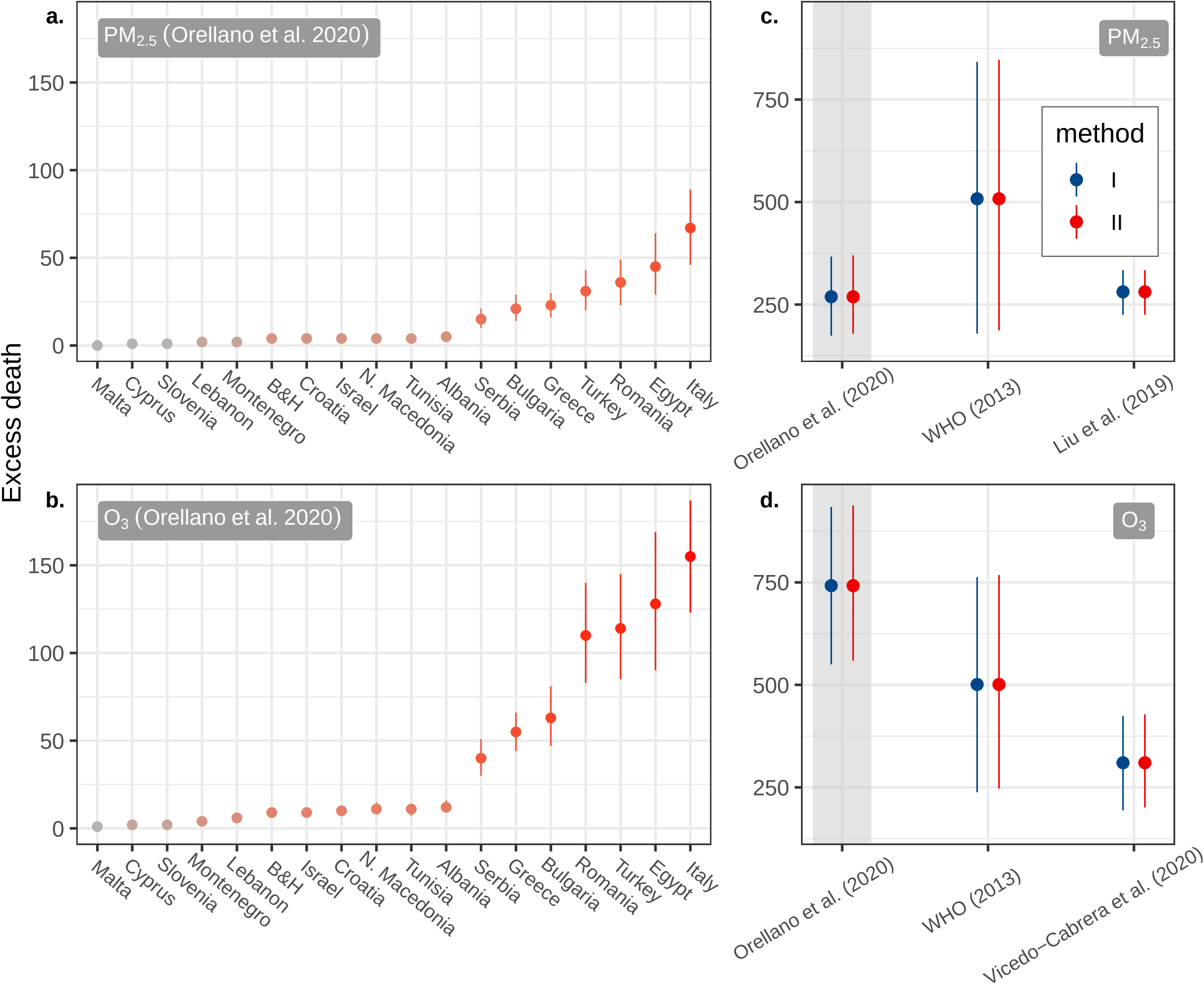

a.
PM$_{2.5}$ (Orellano et al. 2020)
b.
O$_3$ (Orellano et al. 2020)
Excess death
0
50
100
150
Malta
Cyprus
Slovenia
Lebanon
Montenegro
B&H
Croatia
Israel
N. Macedonia
Tunisia
Albania
Serbia
Bulgaria
Greece
Turkey
Romania
Egypt
Italy
c.
PM$_{2.5}$
d.
O$_3$
250
500
750
method
I
II
Orellano et al. (2020)
WHO (2013)
Liu et al. (2019)
Vicedo–Cabrera et al. (2020)

Supplementary Information for

An estimate of excess mortality resulting from air pollution caused by wildfires in the eastern and central Mediterranean basin in 2021

Bin Zhou[1,2], Christoph Knote[1]

[1]Model-based Environmental Exposure Science, Faculty of Medicine, University of Augsburg, Augsburg, Germany

[2]Potsdam Institute for Climate Impact Research (PIK), Member of the Leibniz Association, Potsdam, Germany

Contents of this file

Tables

Figures

- Figure S5: Spatial pattern of multi-month mean NO_2 concentration simulated by WRF-Chem under the fires scenario and the difference relative to the no-fires scenario.
- Figure S6:Spatial pattern of multi-month mean SO_2 concentration simulated by WRF-Chem under the fires scenario and the difference relative to the no-fires scenario.
- Figure S7:Spatial pattern of multi-month mean hydroxyl radical (OH) concentration simulated by WRF-Chem under the fires scenario and the difference relative to the no-fires scenario.
- Figure S8: Diurnal pattern of multi-month hourly mean ambient $PM_{2.5}$ concentration for each country and the entire region of interest.
- Figure S9: Diurnal pattern of multi-month hourly mean O_3 concentration for each country and the entire region of interest.
- Figure S10: Diurnal pattern of multi-month hourly mean SO_2 concentration for each country and the entire region of interest.
- Figure S11: Diurnal pattern of multi-month hourly mean NO_2 concentration for each country and the entire region of interest.
- Figure S12: Time series of 24-h-mean population weighted $PM_{2.5}$ for each country.
- Figure S13: Time series of population weighted daily maximum 8-h average (DMA8) of O_3 for each country
- Figure S14:Time series of 24-h-mean population weighted SO_2 for each country.
- Figure S15: Time series of 24-h-mean population weighted NO_2 for each country.

References

Eurostat. (2021). *Deaths (total) by month, 2010-2019.* Luxembourg.

Global Burden of Disease Collaborative Network. (2020). *Global Burden of Disease Study 2019 (GBD 2019) Results.* Seattle, United States: Institute for Health Metrics and

Evaluation (IHME). Retrieved from http://ghdx.healthdata.org/gbd-results-tool?params=gbd-api-2019-permalink/4e1860d6fad20ccf64c5e6f7e1f7a24b

Holzinger, R., Wameke, C., Hansel, A., Jordan, A., Lindinger, W., Scharffe, D. H., ... Crutzen, P. J. (1999). Biomass burning as a source of formaldehyde, acetaldehyde, methanol, acetone, acetonitrile, and hydrogen cyanide. *Geophysical Research Letters*, *26*(8), 1161–1164. doi: 10.1029/1999GL900156

Kroll, J. H., Heald, C. L., Cappa, C. D., Farmer, D. K., Fry, J. L., Murphy, J. G., & Steiner, A. L. (2020). The complex chemical effects of COVID-19 shutdowns on air quality. *Nature Chemistry*, *12*(9), 777–779. doi: 10.1038/s41557-020-0535-z

Manning, M. I., Martin, R. V., Hasenkopf, C., Flasher, J., & Li, C. (2018). Diurnal Patterns in Global Fine Particulate Matter Concentration. *Environmental Science and Technology Letters*, *5*(11), 687–691. doi: 10.1021/acs.estlett.8b00573

World Bank. (2020). *Total population.* The World Bank Group. Retrieved from https://data.worldbank.org/indicator/SP.POP.TOTL(Accessed11Dec.2021)

	name	ISO-2	ISO-3	pop. (in Mio.)
1	Albania	AL	ALB	2.84
2	Bosnia and Herzegovina (B&H)	BA	BIH	3.28
3	Bulgaria	BG	BGR	6.93
4	Cyprus	CY	CYP	1.21
5	Egypt	EG	EGY	102.33
6	Greece	GR	GRC	10.72
7	Croatia	HR	HRV	4.05
8	Israel	IL	ISR	9.22
9	Italy	IT	ITA	59.55
10	Lebanon	LB	LBN	6.83
11	Montenegro	ME	MNE	0.62
12	North Macedonia (N. Macedonia)	MK	MKD	2.07
13	Malta	MT	MLT	0.53
14	Romania	RO	ROU	19.29
15	Serbia	RS	SRB	6.91
16	Slovenia	SI	SVN	2.10
17	Tunisia	TN	TUN	11.82
18	Turkey	TR	TUR	84.34
	SUM			334.62

Table S1. Countries included in the study and their respective population in 2020, obtained from the World Bank's World Development Indicators database (World Bank, 2020).

	$PM_{2.5}$		O_3	
Country	Method I	Method II	Method I	Method II
Albania	5 [3,7]	5 [3,8]	12 [9,16]	12 [9,16]
B&H	4 [2,6]	4 [3,6]	9 [7,12]	9 [7,12]
Bulgaria	21 [13,29]	21 [14,29]	63 [46,80]	63 [47,81]
Croatia	4 [3,6]	4 [3,6]	10 [7,12]	10 [7,13]
Cyprus	1 [0,1]	1 [0,1]	2 [1,2]	2 [1,2]
Egypt	45 [27,63]	45 [29,64]	128 [88,167]	128 [90,169]
Greece	23 [16,30]	23 [16,30]	55 [43,67]	55 [44,67]
Israel	4 [2,5]	4 [2,5]	9 [7,11]	9 [7,11]
Italy	67 [46,89]	67 [46,89]	155 [123,188]	155 [123,187]
Lebanon	2 [2,3]	2 [2,3]	6 [5,7]	6 [5,7]
Malta	0 [0,1]	0 [0,1]	1 [1,1]	1 [1,1]
Montenegro	2 [1,2]	2 [1,2]	4 [3,5]	4 [3,5]
N. Macedonia	4 [3,6]	4 [3,6]	11 [8,15]	11 [8,15]
Romania	36 [23,48]	36 [23,49]	110 [81,139]	110 [83,140]
Serbia	15 [9,21]	15 [10,21]	40 [29,51]	40 [29,51]
Slovenia	1 [1,1]	1 [1,1]	2 [2,3]	2 [2,3]
Tunisia	4 [3,6]	4 [3,6]	11 [7,14]	11 [7,14]
Turkey	31 [19,43]	31 [20,43]	114 [83,144]	114 [85,145]
SUM	270 [174,367]	270 [177,370]	741 [548,934]	741 [556,940]

Table S2. Excess number of deaths for individual countries and the entire region estimated based on wildfires-caused $PM_{2.5}$ and O_3 loads within the simulation period, with 95% confidence intervals (CIs) in brackets. The methods I and II refer to the Delta and Monte Carlo methods for the uncertainty estimation, respectively, which are described in details in Section 2.4.3 in the main text. The Delta method slightly underestimate the excess deaths compared to the Monte Carlo method. However, the difference is not significant.

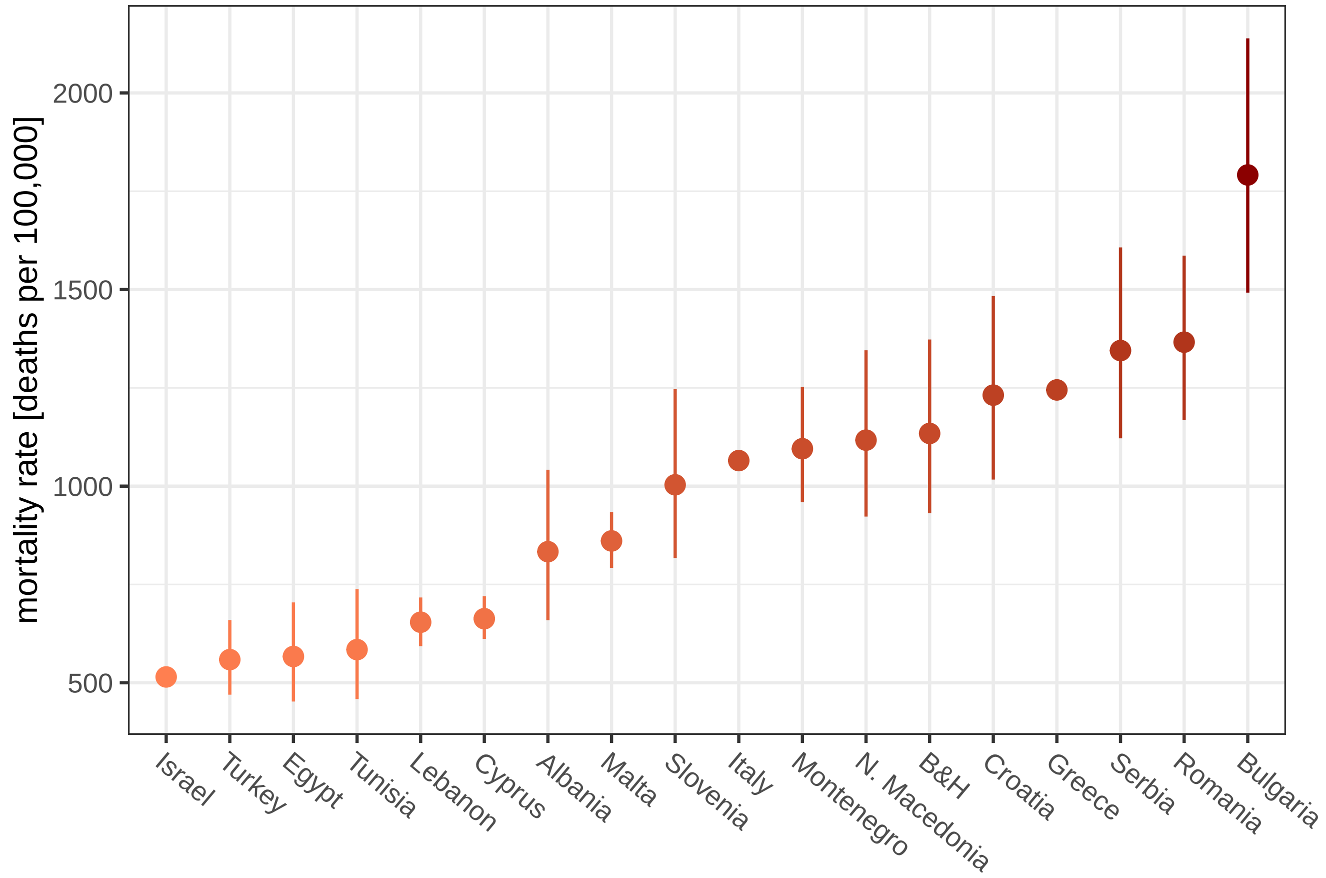

Figure S1. Baseline all-cause mortality in both genders 2019 for each country with 95% confidence intervals, downloaded from the Global Health Data Exchange (Global Burden of Disease Collaborative Network, 2020).The annual mortality rates of countries range from 515 (Israel) to 1791 (Bulgaria) deaths per 100,000 population. B&H stands for Bosnia and Herzegovina.

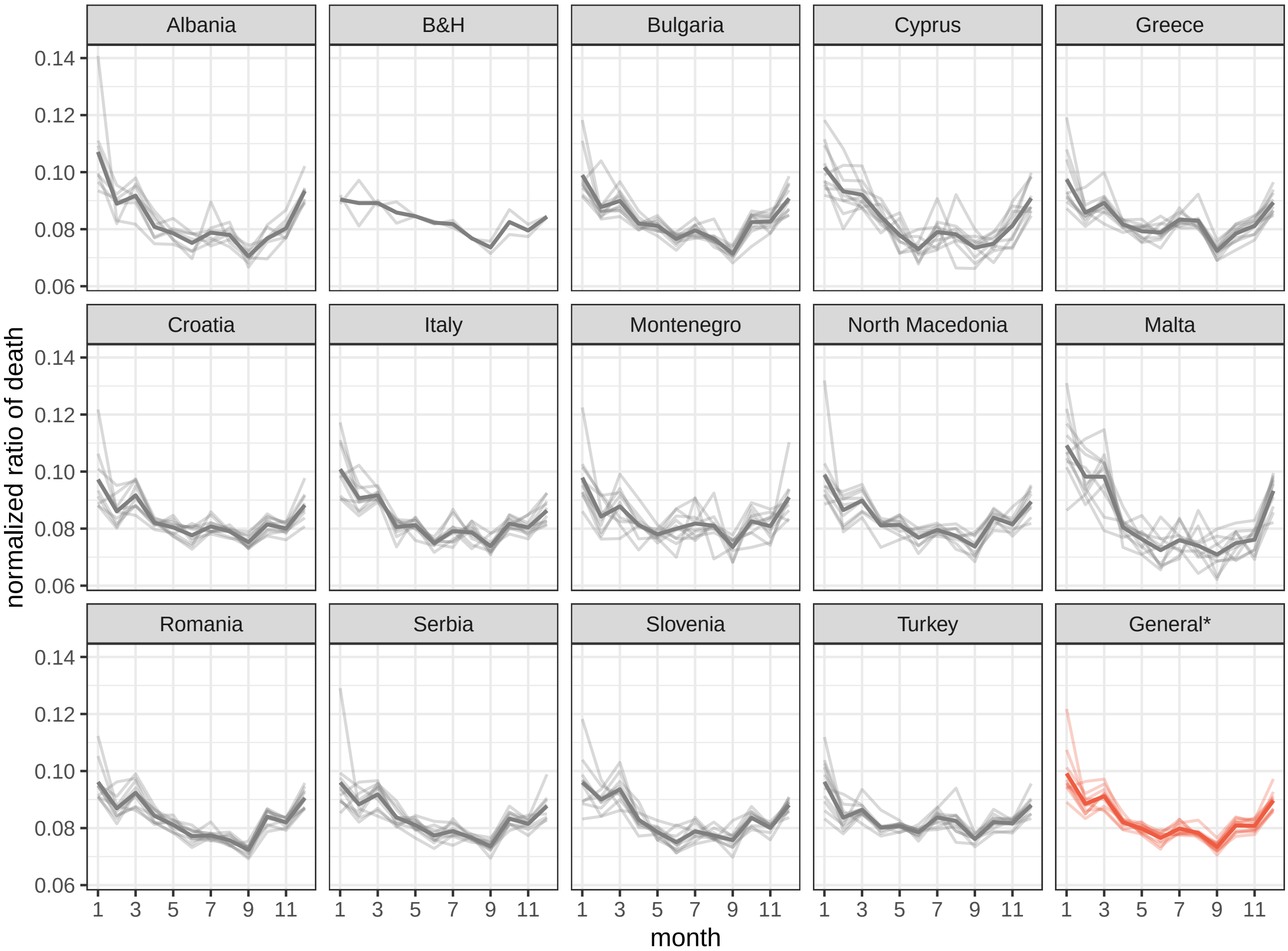

Figure S2. Multi-annual monthly mean normalized ratio of death averaged across 2010-2020 (dark gray, bold), underlaid with data for individual years (light gray) downloaded from (Eurostat, 2021). For countries where monthly death data are not available (e.g., Egypt, Israel, Lebanon), the monthly mortality is calculated based on the regional mean value averaged across all other countries (General*).

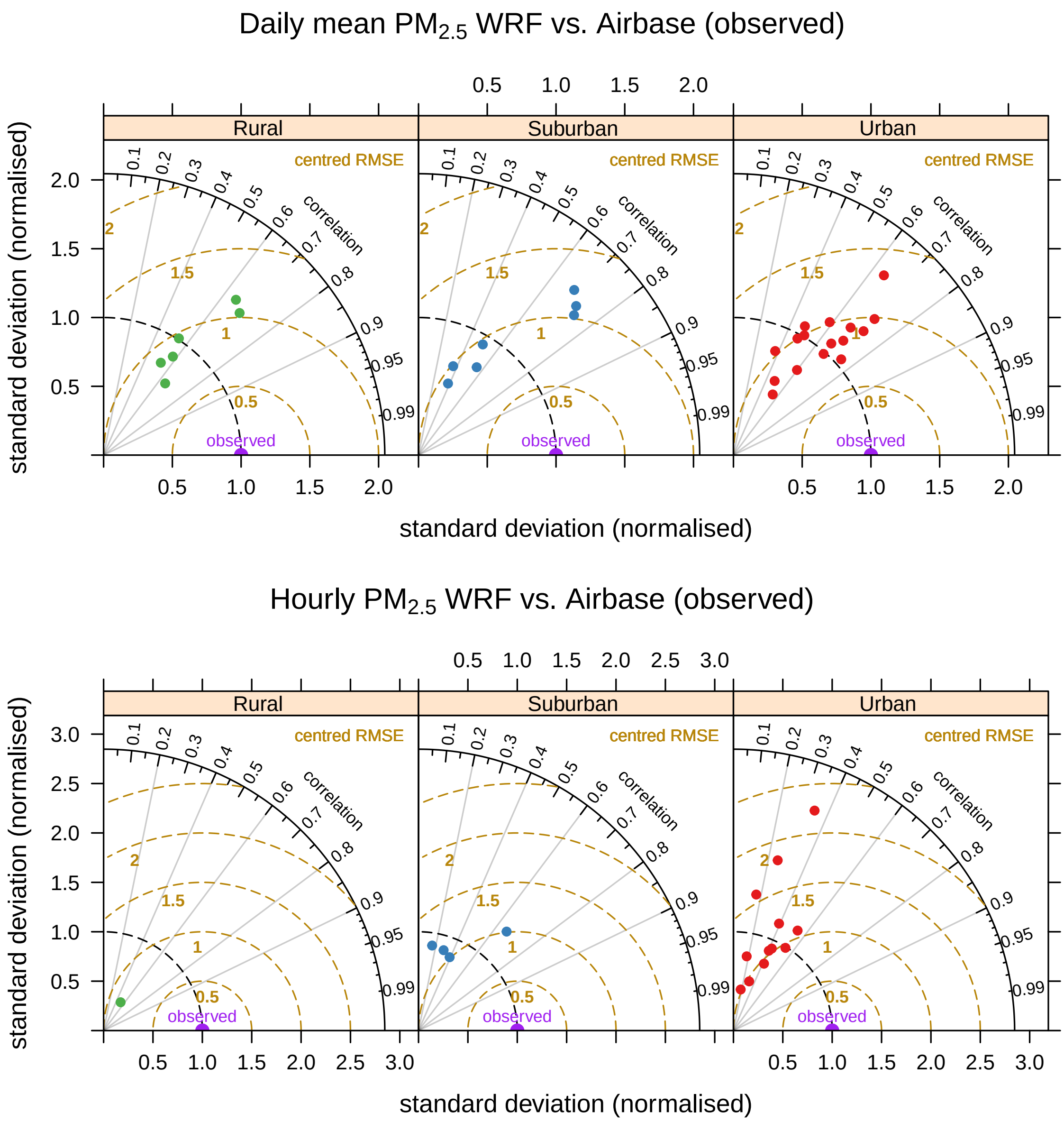

Figure S3. Validation of $PM_{2.5}$ concentration simulated by WRF-Chem using AirBase E1a & E2a air quality data. We only used the verified AirBase data with "verification code" equal to 1 (verified) or 2 (preliminary verified) in the metadata, and data from stations where more than 75% of observations are present during the entire period. Each AirBase station is spatially matched to a WRF grid cell (20 km). The hourly WRF values are also averaged to daily means for comparison with AirBase data from stations where only daily means were recorded.

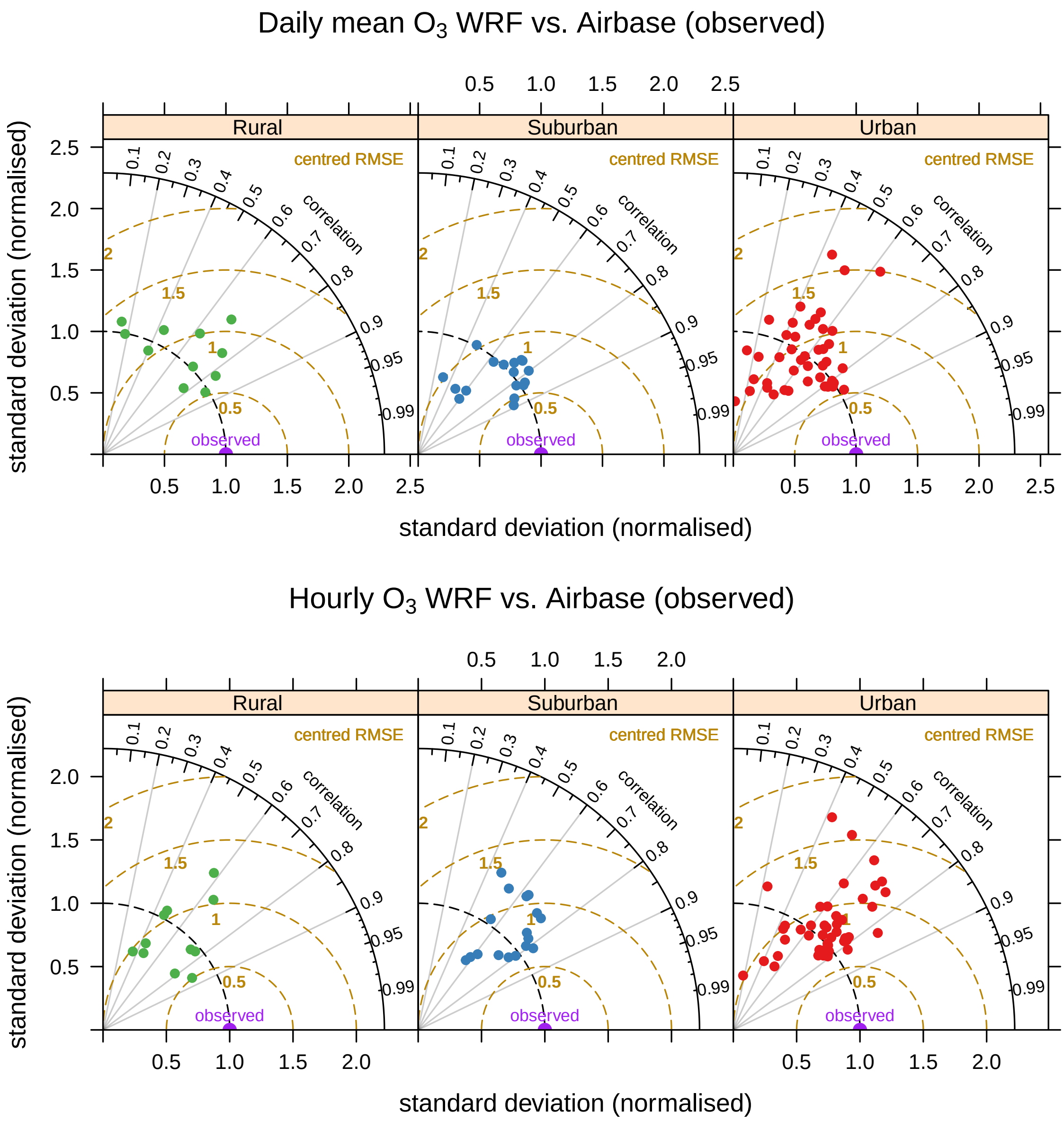

Figure S4. Validation of O_3 concentration simulated by WRF-Chem using AirBase data.

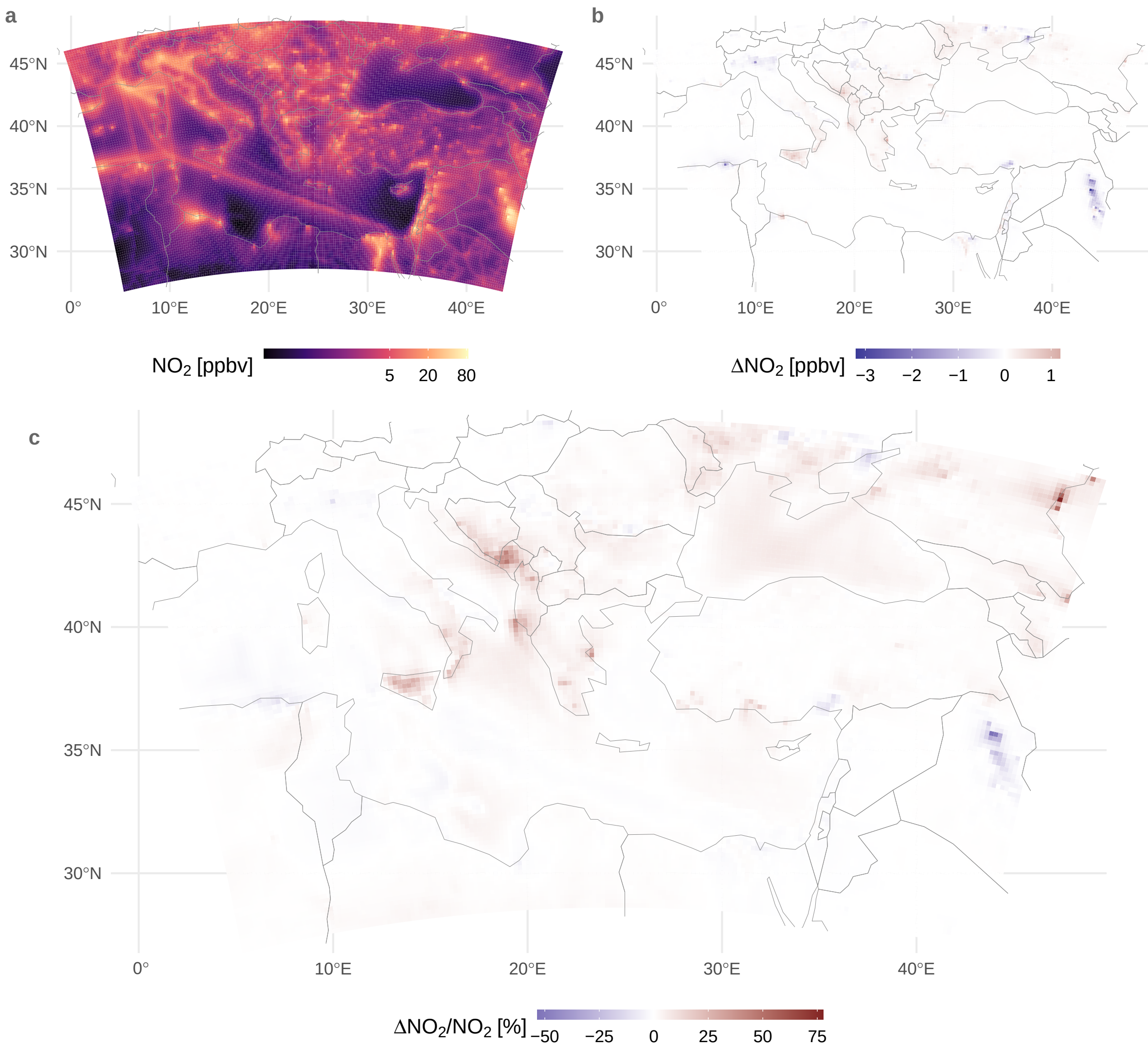

Figure S5. Spatial pattern of multi-month mean NO_2 concentration simulated by WRF-Chem under the fires scenario and the difference relative to the no-fires scenario. a) NO_2 concentration simulated with fires scenario, b) NO_2 concentration with fires scenario relative to no-fires ($\Delta NO_2 = NO_2^{\text{fires}}$- $NO_2^{\text{no-fires}}$), c) NO_2 concentration attributable to wildfires in percentages ($\Delta NO_2/NO_2^{\text{fires}}$).The elevation of wildfire-caused NO_2 is mainly observed in the Balkans, South Italy, and southern coast of Turkey. In contrast, regions with high background industrial pollution show a slight decrease in ambient NO_2 concentration.

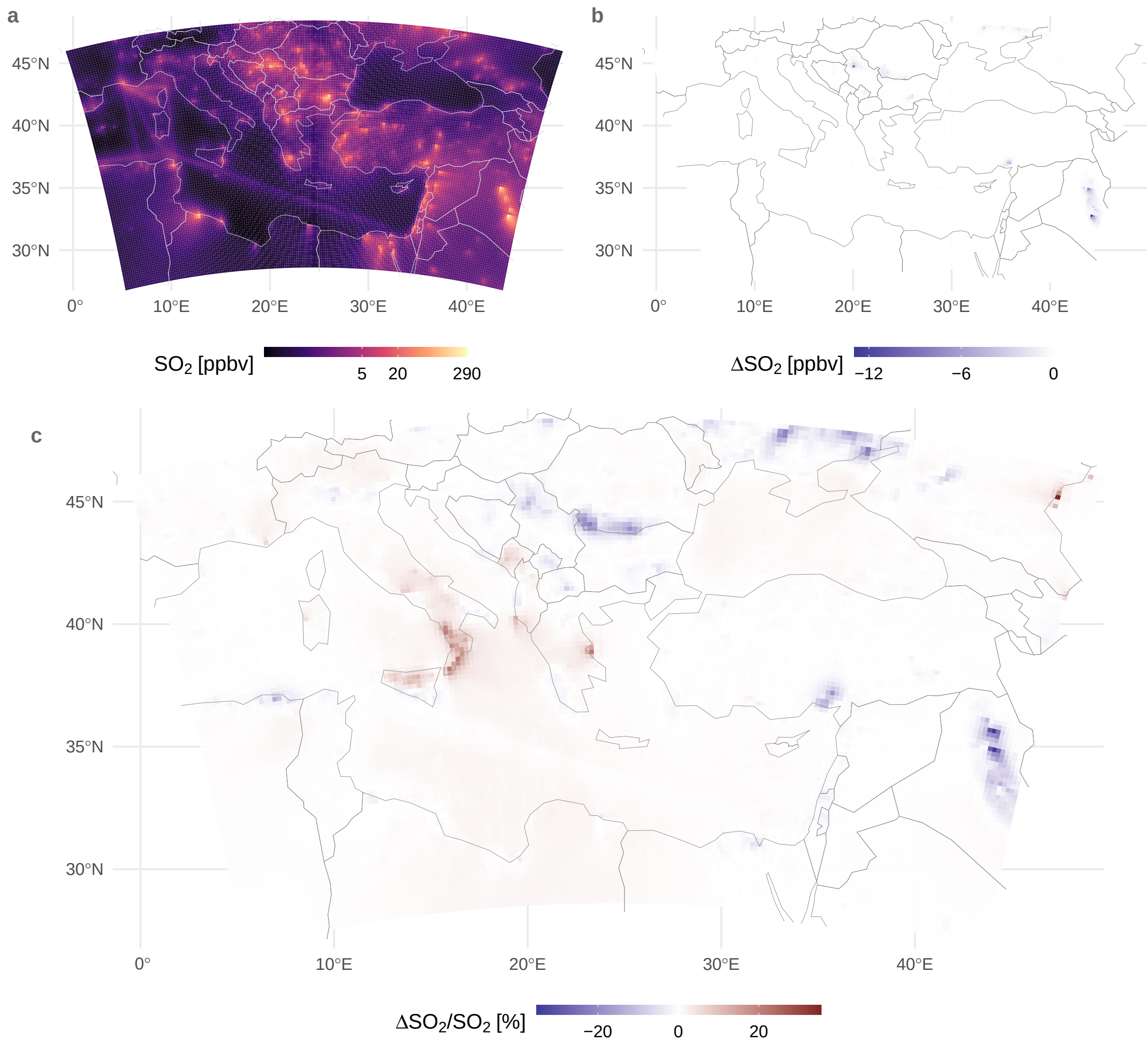

Figure S6. Spatial pattern of multi-month mean SO_2 concentration simulated by WRF-Chem under the fires scenario and the difference relative to the no-fires scenario. a) SO_2 concentration simulated with fires scenario, b) SO_2 concentration with fires scenario relative to no-fires ($\Delta SO_2 = {SO_2}^{\text{fires}}$- ${SO_2}^{\text{no-fires}}$), c) SO_2 concentration attributable to wildfires in percentages ($\Delta SO_2/{SO_2}^{\text{fires}}$).

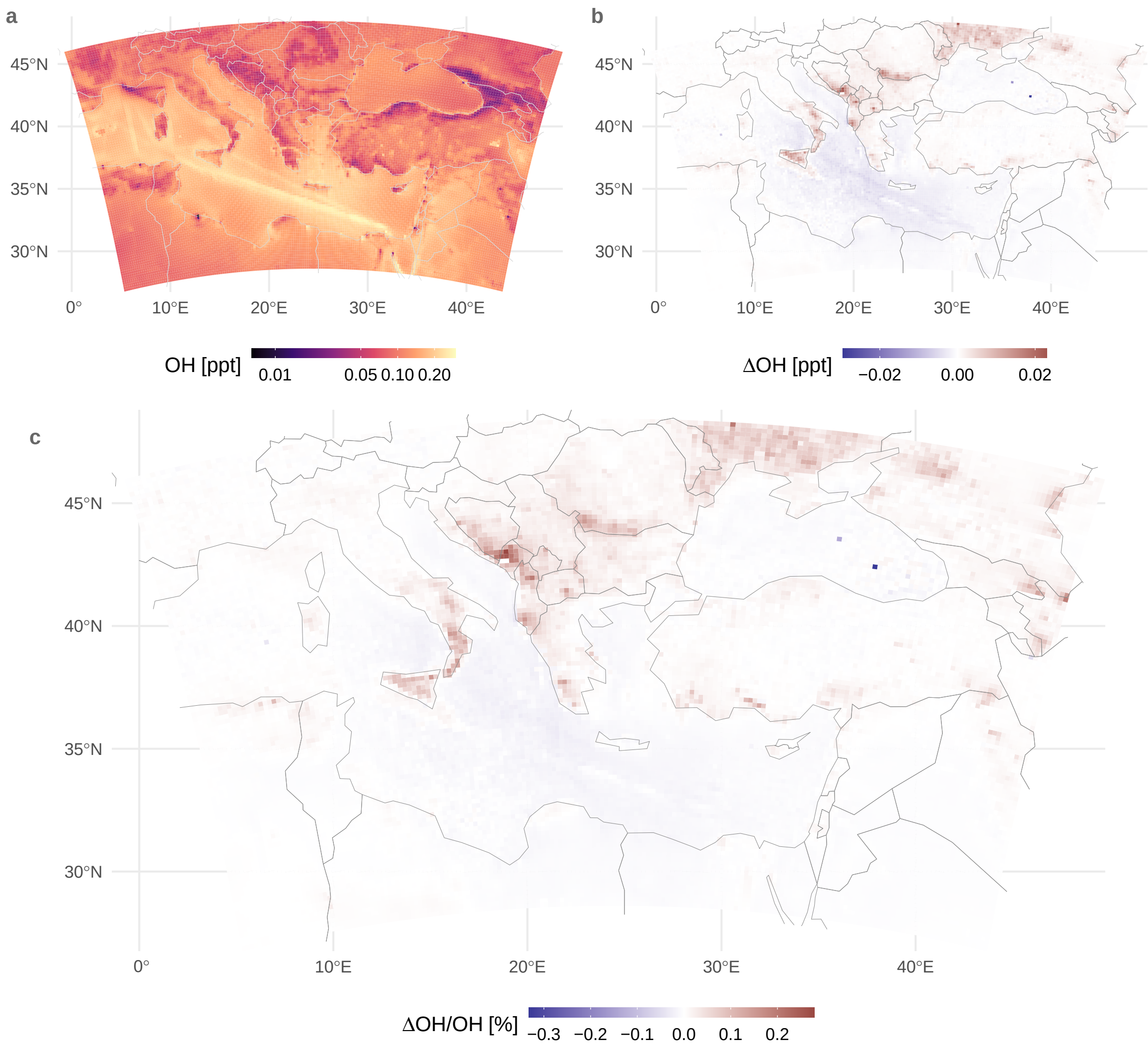

Figure S7. Spatial pattern of multi-month mean hydroxyl radical (OH) concentration simulated by WRF-Chem under the fires scenario and the difference relative to the no-fires scenario. a) OH concentration simulated with fires scenario, b) OH concentration with fires scenario relative to no-fires (ΔOH= OH$^{\text{fires}}$- OH$^{\text{no-fires}}$), c) OH concentration attributable to wildfires in percentages (ΔOH/OH$^{\text{fires}}$).

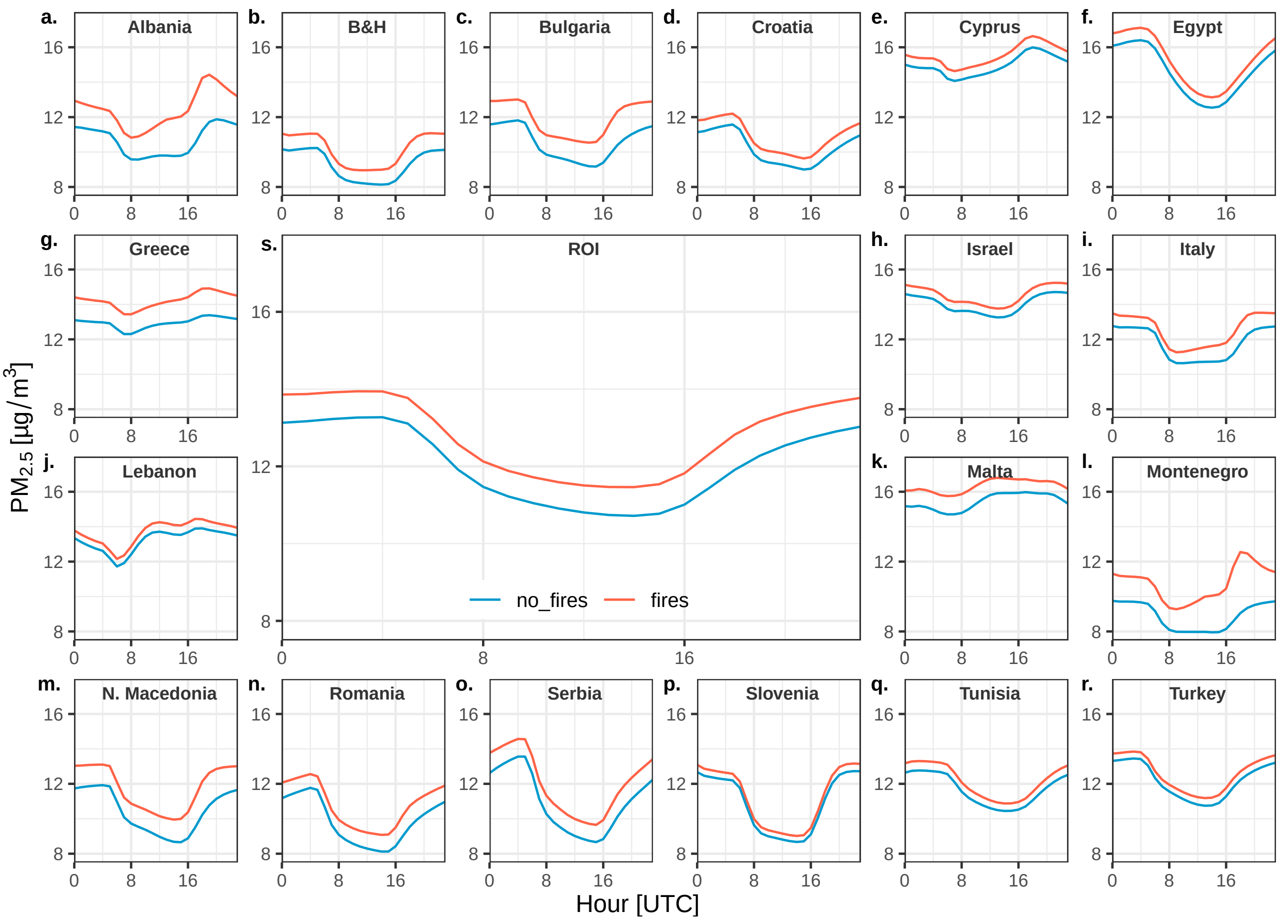

Figure S8. Diurnal pattern of multi-month hourly mean ambient $PM_{2.5}$ concentration for each country and the entire region of interest (ROI). In most countries, the $PM_{2.5}$ concentration follows a pattern subject to the mixing layer height. The daytime troughs reflect strong turbulent exchange and dilution within the mixed layer, whereas stable nighttime boundary layer enables $PM_{2.5}$ to accumulate (Manning et al., 2018). The wildfire-caused elevation of $PM_{2.5}$ concentration in all countries can be ascribed to the emissions of gas-phase air pollutants such as NO_x, and VOCs from wildfires. These species are oxidized to form less volatile nitrates, and secondary organic aerosols (SOAs), respectively, and condense into the particle phase (Kroll et al., 2020).

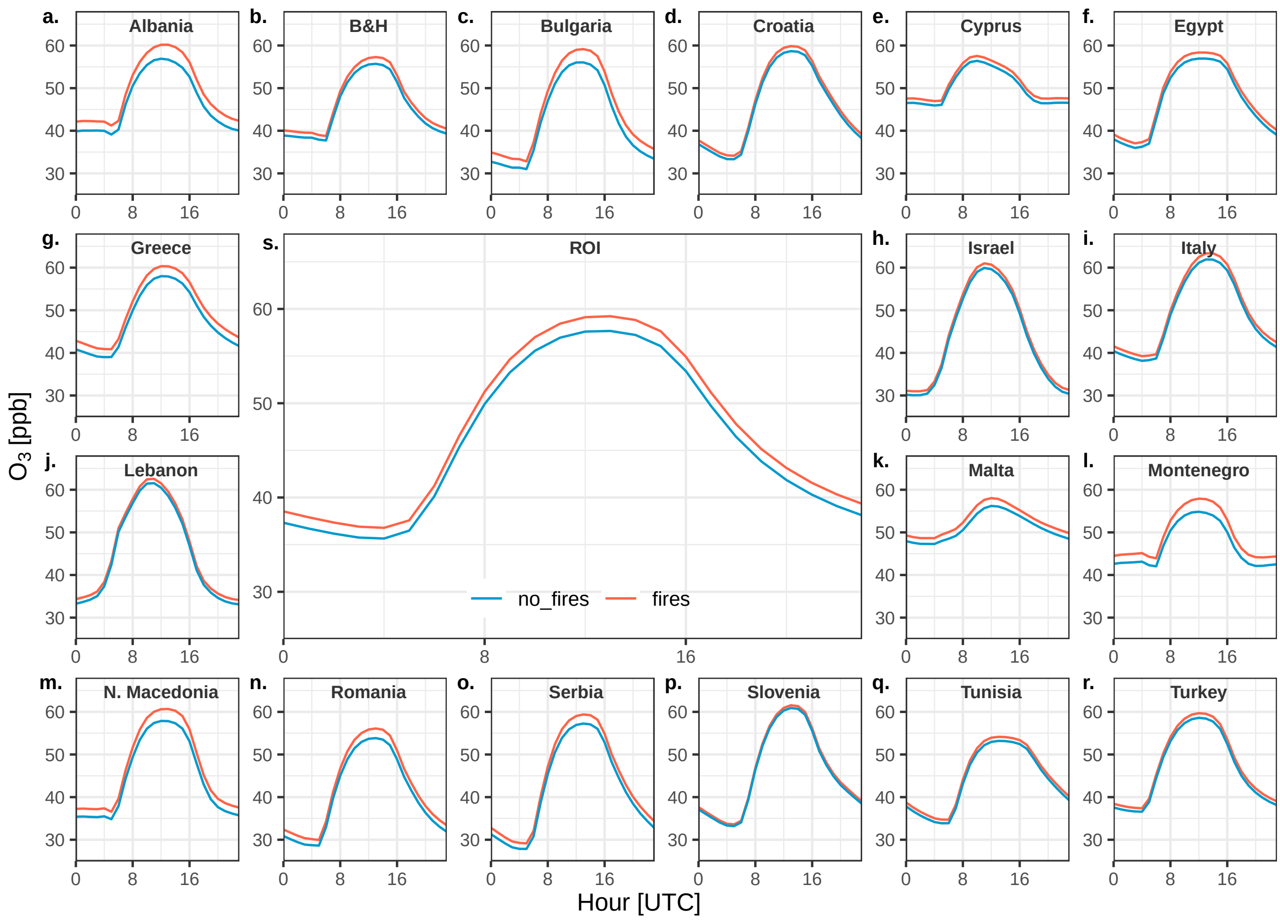

Figure S9. Diurnal pattern of multi-month hourly mean O_3 concentration for each country and the entire ROI. The biomass burning presents a significant source of O_3 precursors such as carbon monoxide (CO), volatile organic compounds (VOCs), and nitrogen oxide (NO_x), which form O_3 in the presence of solar radiation (Holzinger et al., 1999). Therefore, the concentration of O_3 starts to increase after the sunrise and often reaches its maximum in the afternoon (between LT1200 and 1600). As the time of the day (horizontal axis) is in UTC, the local time (LT) of each country may be offset, subject to the time zone which the country is located in.

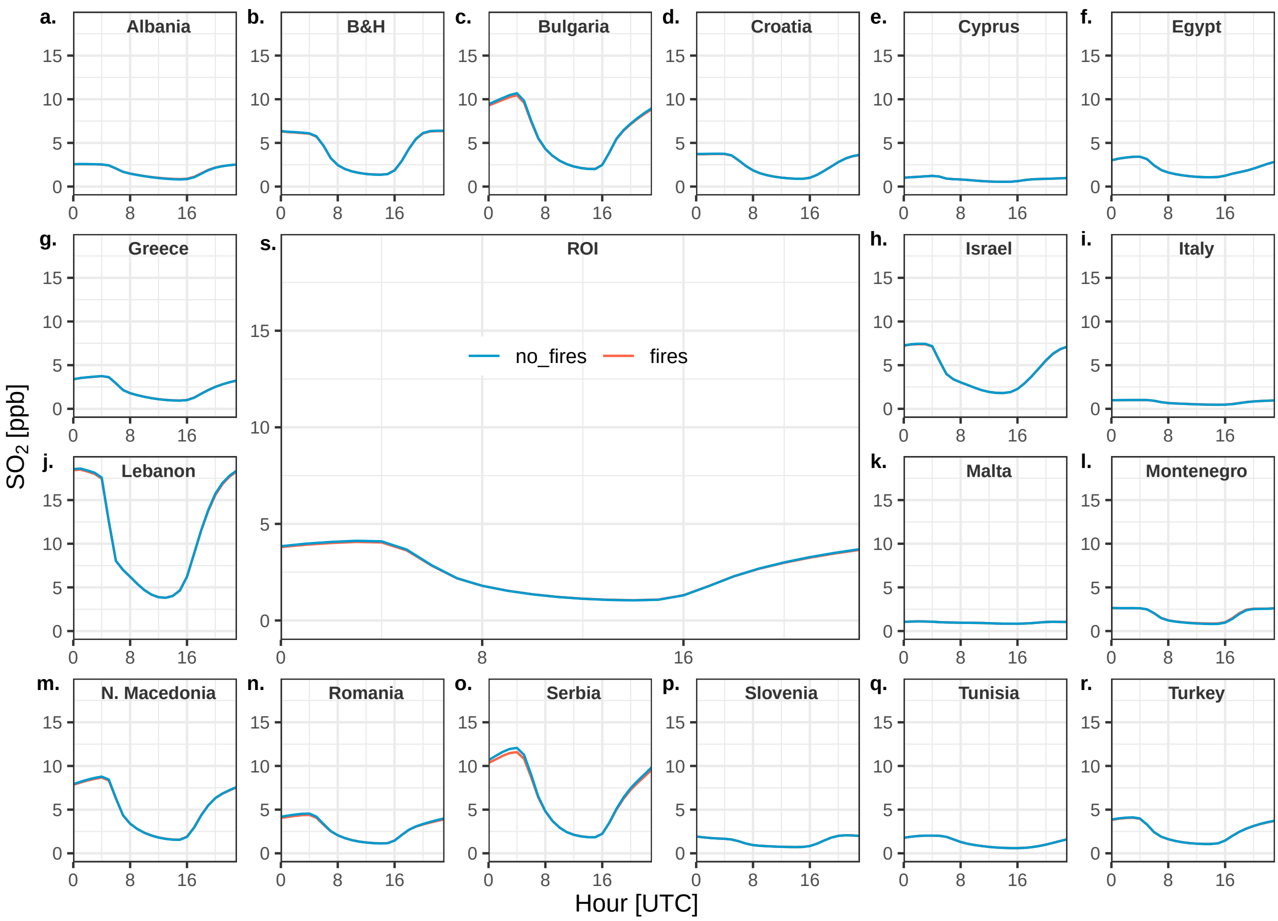

Figure S10. Diurnal pattern of multi-month hourly mean SO_2 concentration for each country and the entire region of interest.

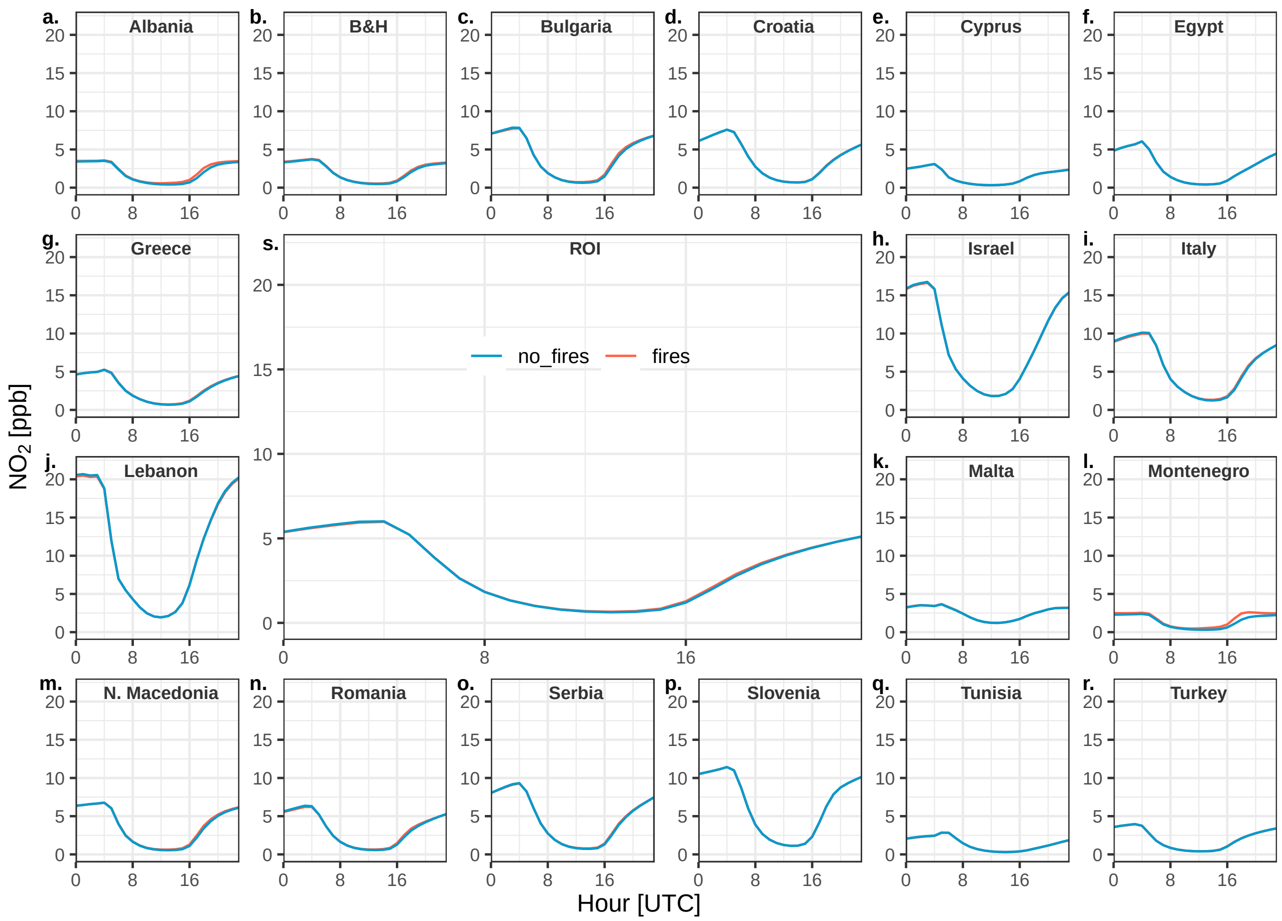

Figure S11. Diurnal pattern of multi-month hourly mean NO_2 concentration for each country and the entire region of interest.

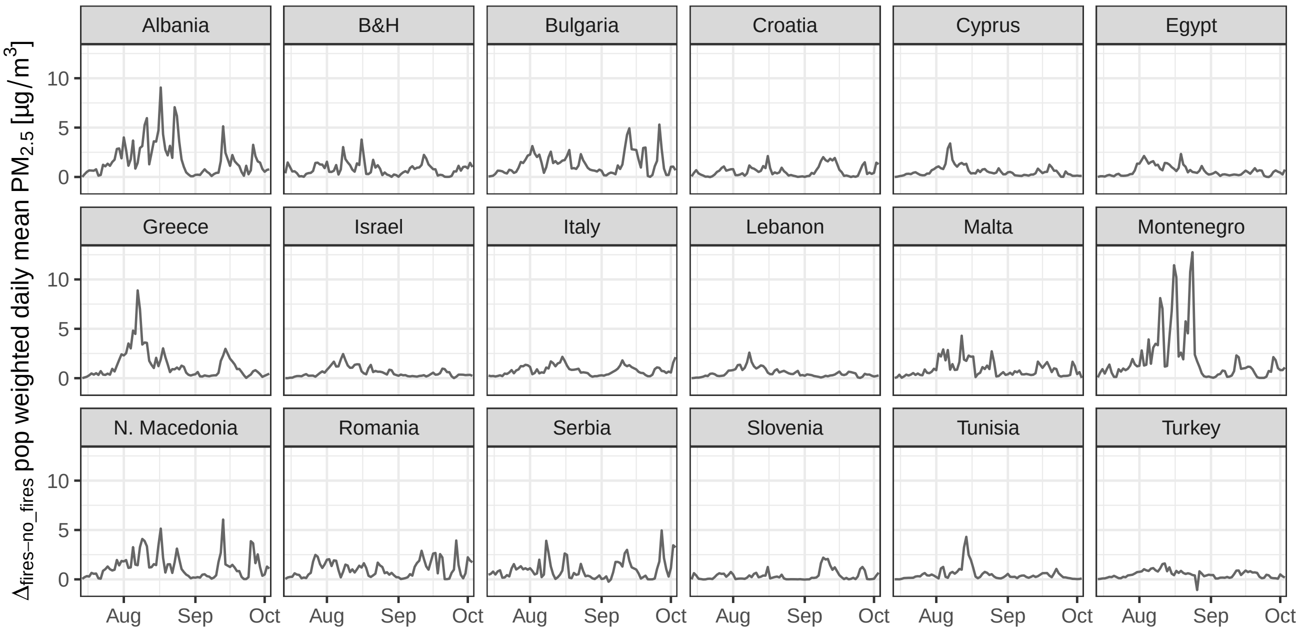

Figure S12. Time series of 24h-mean population weighted concentration of $PM_{2.5}$ for each country.

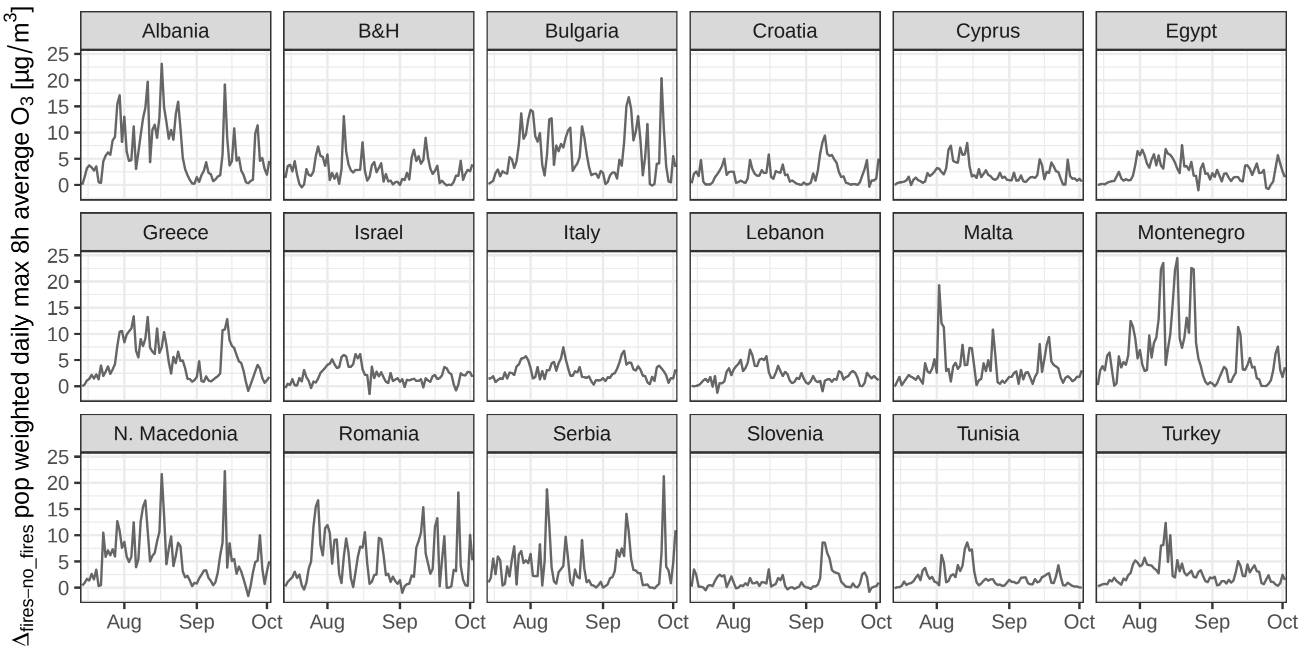

Figure S13. Time series of population weighted daily maximum 8-h average (DMA8) of O_3 for each country.

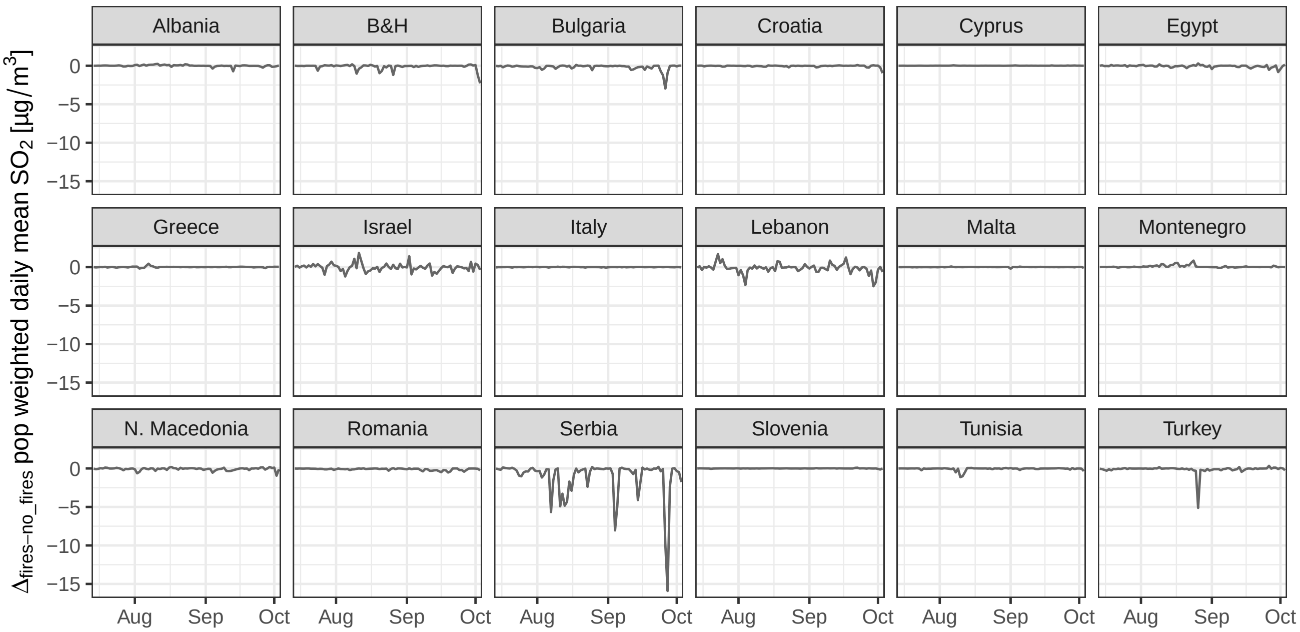

Figure S14. Time series of 24h-mean population weighted concentration of SO_2 for each country.

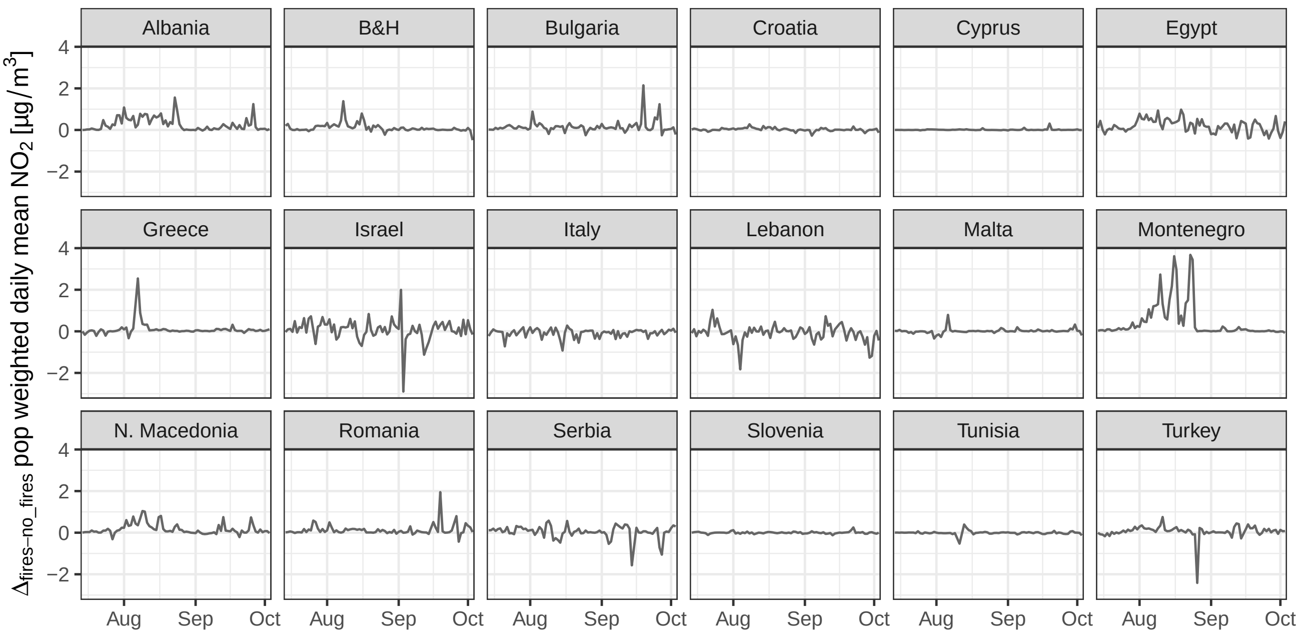

Figure S15. Time series of 24h-mean population weighted concentration of NO_2 for each country.